

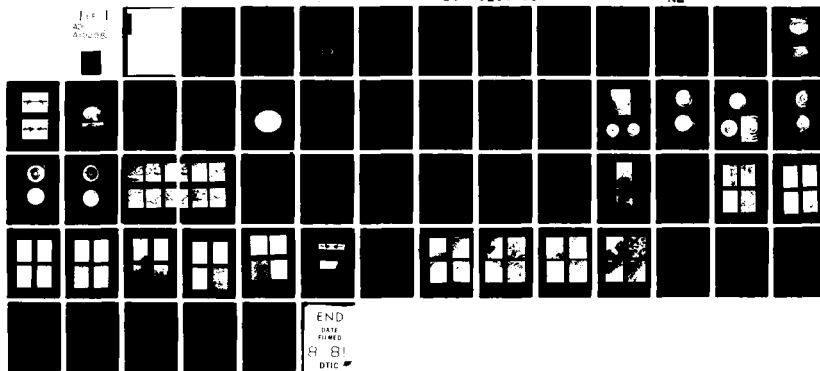
AD-A102 082

PRATT AND WHITNEY AIRCRAFT GROUP WEST PALM BEACH FL 6-ETC F/6 21/5
SHOCK WAVE THERMOMECHANICAL PROCESSING OF GAS TURBINE DISKS. (U)
NOV 80 J M ROBERTSON, J W SIMON, T D TILLMAN N62269-79-C-0281
PWA-FR-13925 NADC-79105-60 NI

UNCLASSIFIED

NADC-79105-60

1820



END
DATE
FILED
8 8
DTIC

ADA102082

UNCLASSIFIED

19 111183-60

SECURITY CLASSIFICATION OF THIS PAGE (When Data Entered)

REPORT DOCUMENTATION PAGE		READ INSTRUCTIONS BEFORE COMPLETING FORM
1. REPORT NUMBER 18) NADC 79105-60	2. GOVT ACCESSION NO. AD-A202,083	3. RECIPIENT'S CATALOG NUMBER
4. TITLE (and Subtitle) 6) SHOCK WAVE THERMOMECHANICAL PROCESSING OF GAS TURBINE DISKS.		5. TYPE OF REPORT & PERIOD COVERED Final Report 1 Aug 1979 through 30 Nov 1980
7. AUTHOR(s) 10) J.M. Robertson, J.W. Simon, T.D. Tillman		6. PERFORMING ORG. REPORT NUMBER -FR-13925
9. PERFORMING ORGANIZATION NAME AND ADDRESS Pratt & Whitney Aircraft P.O. Box 2691 West Palm Beach, FL 33402		10. PROGRAM ELEMENT, PROJECT, TASK AREA & WORK UNIT NUMBERS 11) 31
11. CONTROLLING OFFICE NAME AND ADDRESS Naval Air Development Center Warminster, PA 18974		12. REPORT DATE November 1980
14. MONITORING AGENCY NAME & ADDRESS (if different from Controlling Office) Naval Air Systems Command Department of the Navy Washington, DC 20361		13. NUMBER OF PAGES 15. SECURITY CLASS. (of this report) Unclassified
15a. DECLASSIFICATION/DOWNGRADING SCHEDULE		
16. DISTRIBUTION STATEMENT (of this Report) Approved for public release; distribution unlimited		
17. DISTRIBUTION STATEMENT (of the abstract entered in Block 20, if different from Report)		
18. SUPPLEMENTARY NOTES		
19. KEY WORDS (Continue on reverse side if necessary and identify by block number)		
20. ABSTRACT (Continue on reverse side if necessary and identify by block number) This program involved a study of the effects of two shock wave thermomechanical processing (TMP) schedules on the microstructure, hardness, elevated temperature low-cycle fatigue, stress-rupture, and tensile properties of IN-100 (MOI) gas turbine disk alloy. Peak shocking pressures of 10,000 MPa (1450 ksi 100 kbar) for TMP Schedule I and 15,000 MPa (2175 ksi 150 kbar) for TMP Schedule II were established on subscale sonic-shaped turbine disks.		

UNCLASSIFIED

SECURITY CLASSIFICATION OF THIS PAGE (When Data Entered)

These pressures were applied to flat plates of the respective schedules for mechanical property evaluations. In general, processing according to TMP Schedules I and II contributed only minor strength improvements, with a corresponding loss in ductility. Strength increases were attributed to the complex dislocation substructure created by the shock wave treatments. No significant improvement in low-cycle fatigue life was noted for either shock schedule. Stress-rupture testing showed no improvement over conventionally processed IN-100 for either schedule, and results indicated an increase in the notch sensitivity of IN-100 due to shocking. Microstructures appeared unaffected by processing schedule in optical microscopy examinations. Transmission electron microscopy studies revealed a higher dislocation density in disks shocked according to Schedule II than Schedule I. The shocking stage in both schedules prevented ripening of primary cooling γ' on subsequent postshock heat treatments. Postshock heat treatments promoted dislocation recovery, although no real cellular substructure was observed.

S N 0102- LF- 014- 6601

UNCLASSIFIED

SECURITY CLASSIFICATION OF THIS PAGE (When Data Entered)

FOREWORD

This report describes work accomplished by the Materials Engineering and Technology Department of the Government Products Division of Pratt & Whitney Aircraft Group for the Naval Air Development Center under Contract No. N62269-79-C-0281. Mr. Irving Machlin served as Program Technical Consultant.

The authors are indebted to the Naval Air Development Center for the opportunity to conduct this investigation and to Mr. Irving Machlin for his encouragement and guidance. The authors also acknowledge the contributions of Dr. J. D. Mote at Denver Research Institute.

DTIC
ELECTED
JUL 27 1981
S B D
A

Accession For	
NTIS	GRAKI <input checked="" type="checkbox"/>
DTIC TAB	<input type="checkbox"/>
Unnumbered	<input type="checkbox"/>
Justification	
By	
Distribution	
Available Title Codes	
Dist	Avail and/or
A	Original

TABLE OF CONTENTS

<i>Section</i>		<i>Page</i>
I	INTRODUCTION	1
II	TECHNICAL BACKGROUND	2
III	EXPERIMENTAL PROCEDURE	4
	Materials	4
	Materials Processing	7
	Metallography	11
	Mechanical Testing	12
IV	RESULTS & DISCUSSION.....	15
	Peak-Pressure Shocking	15
	Mechanical Testing	15
	Microstructural Examinations	30
V	CONCLUSIONS	46
	REFERENCES	47

LIST OF ILLUSTRATIONS

<i>Figure</i>	<i>Page</i>
1. F100B Subscale, Sonic-Shaped Turbine Disk	5
2. TF30 Subscale, Sonic-Shaped Turbine Disk	5
3. F100B Cross Section	6
4. TF30 Cross Section	6
5. Forged IN-100 Flat Plate	7
6. Shock Wave Apparatus, Simulated Plane Wave Generator	9
7. Flat Plate No. 1 — Schedule I, Shocked at 10,000 MPa (1450 ksi/100 kbar)	10
8. Shock Wave Apparatus, Mousetrap Plane Wave Generator	11
9. Strain Control Low-Cycle Fatigue Specimen	13
10. Combination Stress-Rupture Specimen	14
11. Standard Round Bar Tensile Specimen	14
12. F100B Subscale Disk No. 1 — Schedule I, Shocked at 17,500 MPa (2540 ksi/175 kbar)	16
13. F100B Subscale Disk No. 6 — Schedule II, Shocked at 17,500 MPa (2540 ksi/175 kbar)	17
14. TF30 Subscale Disk No. 2 — Schedule II, Shocked at 15,000 MPa (2175 ksi/150 kbar)	18
15. TF30 Subscale Disk No. 7 — Schedule II, Shocked at 15,000 MPa (2175 ksi/150 kbar)	19
16. TF30 Subscale Disk No. 9 — Schedule II, Shocked at 15,000 MPa (2175 ksi/150 kbar)	20
17. TF30 Subscale Disk No. 3 — Schedule I, Shocked at 12,500 MPa (1810 ksi/125 kbar)	21
18. SEM Photographs of Typical Void and Inclusion Low-Cycle Fatigue Fracture Origins	22
19. Low-Cycle Fatigue Test Results	25
20. SEM Photographs — Low-Cycle Fatigue Fracture Origins at Shock Wave Induced Secondary Cracks	29
21. As-Extruded IN-100 Billet Microstructures	31
22. Preshock Heat Treated Disk Microstructures	32
23. As-Shocked Disk Microstructures	33
24. Postshock Heat Treated Disk Microstructures — Control Disks	34
25. Postshock Heat Treated Disk Microstructures	35
26. As-Shocked Flat Plate Microstructures	36
27. Postshocked Heat Treated Flat Plate Microstructures	37
28. Disk No. 8 — Schedule II, Typical Impact Surface Crack	38
29. Preshock Heat Treated Disk — Schedule I	40
30. Postshock Heat Treated Disk — Schedule I	41
31. Preshock Heat Treated Disk — Schedule II	42
32. Postshock Heat Treated Disk — Schedule II	43

LIST OF TABLES

<i>Table</i>		<i>Page</i>
1	Chemical Composition of Homogeneous IN-100 Billet.....	4
2	Disk Shocking Summary	10
3	Mechanical Testing Results of Control Materials	23
4	Mechanical Testing Results of Shock Wave Processed Materials	26
5	Mechanical Properties — Statistical Analysis	28
6	Heat Treatments and Microstructure	39
7	Carbide Size and Distribution	45
8	Dislocation Structure	45

SECTION I

INTRODUCTION

Performance improvements in current gas turbine engines, such as the Pratt & Whitney Aircraft (P&WA) F100 engine, became possible through advancements in design technology and material processing techniques. The investigation of shock wave thermomechanical processing (TMP) of IN-100 turbine disk material at P&WA Government Products Division (GPD) bore such performance improvements in mind. Because F100 turbine disks are limited by low-cycle fatigue (LCF) life, this contract effort was directed toward property enhancements in this area.

This program was sponsored by the Naval Air Development Center (NADC) under Contract No. N62269-79-C-0281, based on the results of Naval Air Systems Command Contract No. N00019-78-C-0280. The previous program examined five shock wave thermomechanical processing schedules. Of these, two schedules appeared most promising and became subject to further investigation in this program.

The approach for this study entailed forging sonic-shaped, subscale turbine disks and flat plates from IN-100 powder extrusions. They were subsequently shock loaded through two TMP schedules. Peak shock wave working pressures were established on the shaped disks from each processing schedule to simulate application to actual engine hardware. These pressures were then applied to flat plates of the respective schedules. A control subscale disk and flat plate were retained for each processing schedule. The respective heat treatments were applied on these materials with the shocking step omitted.

Control materials of each schedule provided physical property baseline data for comparison with the properties of the Schedule I and Schedule II shock wave processed disks and plates. It was necessary to perform these control tests on material from the same lot as the shock wave subscale processed materials in order to eliminate both variable material properties and subscale heat treatment effects.

Control and peak-pressure shocked disks from each schedule underwent mechanical testing and microstructure evaluations, including hardness surveys, optical microscopy, and transmission electron microscopy (TEM) at each stage of processing. The flat plates were used to assess elevated temperature low-cycle fatigue, stress-rupture, and tensile properties, and for hardness surveys and optical microscopy examinations.

This final technical report includes the results of a 15-month effort conducted from 1 August 1979 to 30 November 1980.

SECTION II

TECHNICAL BACKGROUND

Shock wave thermomechanical processing (TMP) has been proven an effective industrial method of hardening and strengthening materials to improve wear resistance. The major usage has been to harden Hadfield manganese steel for railroad trackwork. Additional applications include hardening of structural steels for jaw crushers, ore handling equipment, tread links for power shovels, and cutter teeth for coal mining machines⁽¹⁾.

The technology offers several inherent advantages over the conventional deformation processes of forging and rolling. Most important, parts of irregular shapes, such as turbine disks, may be cold worked without shape or texture change, and with minimal fracture of second phase particles. In terms of mechanical property improvements, shock wave TMP of metal provides both higher hardness levels at a given level of true strain and greater toughness at a given strength level than cold rolling. Appleton and Waddington⁽²⁾ clearly demonstrated this hardening ability for copper, while Peitteiger^(3, 4) achieved better toughness with stainless, nickel, manganese, and carbon steels in the as-shocked versus cold-rolled state.

Hardness and strength improvements are primarily attributed to the high dislocation density of the shocked material.⁽⁵⁾ Evidence also indicates that active slip plane spacing is significantly reduced in shocked materials, which makes the slip process more difficult.⁽⁶⁾ Additional strengthening effects result through dislocation-precipitate interactions and the twinning response observed in shocked microstructures.⁽⁵⁾ Dislocation-precipitate interactions impede dislocation motion, and preshock and/or postshock aging heat treatments may increase this effect. Strength enhancement due to twinning arises from additional dislocations that must be generated to pass a single dislocation through a twinned crystal. This production of dislocations requires energy, and necessarily increases the applied shear stress to move the dislocation.⁽⁵⁾

Since shock wave TMP depends on developing and maintaining a complex dislocation substructure, commercial adaptation has been limited to intermediate temperature applications. However, research in shock deformation has been extended recently to higher temperature materials, particularly nickel-based superalloys. Investigations included alloys AF2-1DA⁽⁵⁾ Inconel 718,^(5, 6) and Udimet 700^(5, 6) in a shocking pressure range of 50,000 to 53,000 MPa (7250 to 7685 ksi/500 to 527 kbars) at a pressure pulse period of 1 microsec.

Mechanical test results show the greatest benefits of shock processing were achieved in the low-cycle fatigue (LCF) and stress-rupture lives of the AF2-1DA alloy at the high shock pressures previously mentioned. Improvements in 760°C (1400°F) LCF life ranged between factors of two and ten over conventionally processed materials, and the 760°C/585 MPa (1400°F 85 ksi) stress-rupture life increased by a factor of five. In comparison, the Inconel 718 and Udimet 700 materials exhibited improvements of only 50 and 78%, respectively in 650°C (1200°F) LCF life. However, while Inconel 718 showed only an 80% improvement in 650°C/690 MPa (1200°F 110 ksi) stress-rupture life, Udimet 700 indicated a two order of magnitude extension in 650°C/830 MPa (1200°F 120 ksi) stress-rupture life.

All three shock treated alloys exhibited tensile property improvements. Yield strength at 650°C (1200°F) increased 25% for both Inconel 718 and Udimet 700. AF2-1DA showed a 15% improvement in 760°C (1400°F) yield strength. In addition, no associated reduction in ductility was observed in any of the alloys. In fact, reduction in area at 650°C (1200°F) increased by 200 and 100% for Inconel and Udimet 700, respectively, while AF2-1DA showed a 15% elevation in the reduction in area.

Shock wave TMP of the IN-100 alloy was investigated in the previous program in the pressure range of 10,000 to 15,000 MPa (1450 to 2175 ksi/100 to 150 kbars) at a pressure pulse period of 1 microsec.¹⁰ Shock wave processing afforded a maximum improvement in IN-100 705°C (1300°F) yield strength of 10 to 11%, although reduction in area decreased between 25 and 35%. LCF test results proved inconclusive. Stress-rupture properties were not evaluated.

SECTION III

EXPERIMENTAL PROCEDURE

MATERIALS

P&WA purchased a 100 kg (220 lb) IN-100 (MOD) billet from Homogeneous Metals Inc. as wrought powder product. The billet measured 17.8 cm (7.0 in.) dia by 51.8 cm (20.0 in.) long. Chemical analysis confirmed the billet to be within the composition limits of the IN-100 PWA 1056 Specification, as shown in Table 1.

TABLE 1. CHEMICAL COMPOSITION
OF HOMOGENEOUS IN-100
BILLET

Element	Weight Percent*
Al	5.15
B	0.025
C	0.083
Co	18.60
Cr	12.55
Cu	0.010
Fe	0.210
Mn	0.02
Mo	3.39
Nb + Ta	0.044
Ni	balance
Si	0.071
Ta	0.023
V	0.72
W	0.02
Bi	0.5 ppm**
Pb	2 ppm**
O	79 ppm***

*Composition determined by quantitative spectroscopy

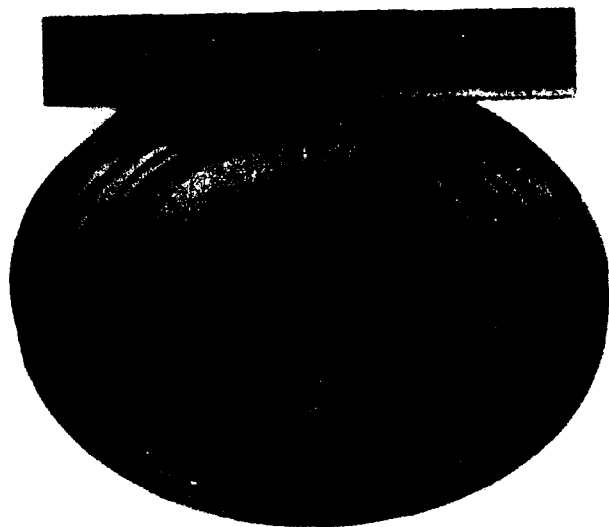
**Composition determined by atomic absorption

***Composition determined by LECO analysis

Subscale Disks

The billet was sectioned into ten pancake preforms of 12.7 cm diameter (5.0 in.) and 2.3 cm (0.9 in.) thickness. Preforms were GATORIZEDTM in a vacuum at 1095 °C (2000 °F) using a 0.25 cm² cm⁻¹ min⁻¹ (0.1 in. in⁻¹ min⁻¹) strain rate to form subscale, sonic-shaped turbine disks.

The original program plan specified ten subscale 1st-stage F100B-type turbine disks, as shown in Figure 1. However, following the forging of the third disk, the F100B die was badly damaged. Because a replacement die was not available for the seven remaining disks, a subscale 1st-stage TF30 turbine disk die was substituted. The remaining seven preforms were forged to the TF30 sonic shape. The TF30 subscale disk, shown in Figure 2, is of the same 16.00 cm (6.30 in.) diameter and 3.00 cm (1.20 in.) maximum thickness as the F100B disk, although the two disks differ in the geometry of their cross section, as shown in Figures 3 and 4.



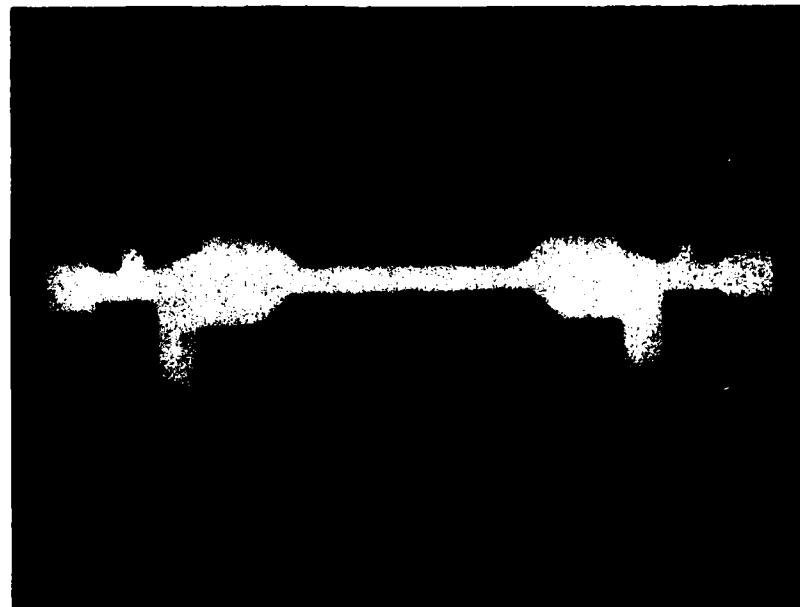
FAL 56503

Figure 1. F100B Subscale, Sonic-Shaped Turbine Disk



FAL 56502

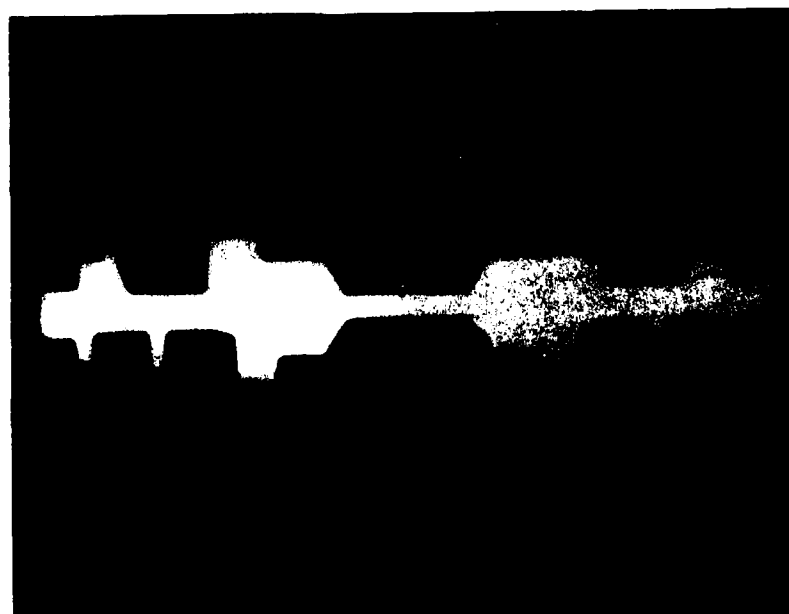
Figure 2. TF30 Subscale, Sonic-Shaped Turbine Disk



Mag. 0.67X

FAI-56926

Figure 3. F100B Cross Section



Mag. 0.67X

FAI-56926

Figure 4. TF30 Cross Section

Flat Plates

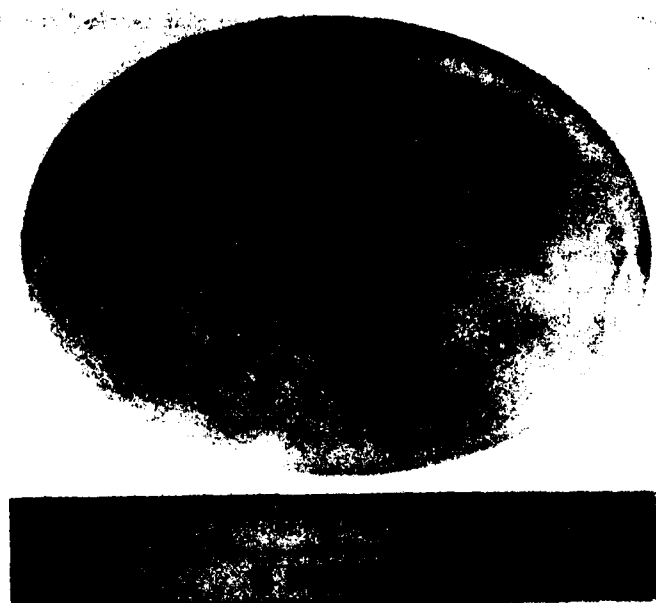
The material remaining from the original IN-100 billet was extruded to a 7.0 cm (2.75 in.) diameter utilizing the following extrusion parameters:

Temperature $1080 \pm 14^\circ\text{C}$ ($1975 \pm 25^\circ\text{F}$)

Reduction in
Area Ratio 6.5:1

Extrusion Rate 5 cm sec (2 in. sec)

The extruded material was machined into eight preforms, 6.1 cm (2.4 in.) in diameter by 8.6 cm (3.4 in.) thick. Each preform was then forged to a 14.5 cm (5.7 in.) dia by 1.5 cm (0.6 in.) thick flat plate, as shown in Figure 5. The forging parameters were identical to those used on the subscale disks.



FAL 58284

Figure 5. Forged IN-100 Flat Plate

MATERIALS PROCESSING

The materials processing of subscale disks and flat plates consisted of the following two shock wave thermomechanical processing schedules:

Schedule I — $1130 \pm 8^\circ\text{C}$ ($2065 \pm 15^\circ\text{F}$) 2hr oil quench + shock + $650 \pm 8^\circ\text{C}$ ($1200 \pm 15^\circ\text{F}$) 24 hr air cool + $760 \pm 8^\circ\text{C}$ ($1400 \pm 15^\circ\text{F}$) 4 hr air cool.

Schedule II — $1130 \pm 8^\circ\text{C}$ ($2065 \pm 15^\circ\text{F}$) 2hr oil quench + $870 \pm 8^\circ\text{C}$ ($1600 \pm 15^\circ\text{F}$) 40 ± 5 min. air cool + $980 \pm 8^\circ\text{C}$ ($1800 \pm 15^\circ\text{F}$) 45 ± 5 min. air cool + shock + $650 \pm 8^\circ\text{C}$ ($1200 \pm 15^\circ\text{F}$) 24 hr air cool + $760 \pm 8^\circ\text{C}$ ($1400 \pm 15^\circ\text{F}$) 4 hr air cool.

Selected on the basis of test results of five IN-100 processing schedules previously examined under NASC Contract No. N00019-78-C-0280, Schedules I and II exhibited the greatest potential for the improvement of LCF life. Results indicated an apparent factor of three improvement in 540°C (1000°F) LCF life.

The peak shocking pressures were established on disks from each schedule. These pressures were then applied to flat plates of their respective schedules. Three flat plates from each schedule underwent preshock heat treat, shocking at the peak pressure, and post-shock heat treat. Plates were then subjected to mechanical property and microstructure examinations.

Heat Treatment

Two heat treatments were associated with TMP Schedules I and II. Schedule II materials were heat treated in accordance with the standard PWA 1073 specification currently used on production IN-100 turbine disks. Schedule I materials were heat treated in accordance with the PWA 1073 specification, except the 870°C (1600°F) and 980°C (1800°F) stress relief cycles were omitted. This heat treatment was originally examined in the previous program to evaluate the effects of γ' precipitation from a solution and shocked structure.

The shocking stage was interjected into both heat treat cycles immediately prior to the low temperature γ' and final age (650°C [1200°F] and 760°C [1400°F] heat treatments, respectively). Shocking, directly preceded these low temperature cycles to minimize thermal recovery and to retain the beneficial effects of shocking.

Disk and flat plate materials underwent heat treatment in accordance with current IN-100 disk production practice. Heat treatments were performed in an air atmosphere with temperature monitored by Type K Inconel-sheath thermocouples located at the disk/plate rim. Materials were quenched in Gulf Superquench 70 oil at 27°C (80°F). The γ' and final ages were accomplished using a Lindberg electric pit furnace.

Shock Wave Loading

Denver Research Institute (DRI), under the direction of Pratt & Whitney Aircraft, performed the shock wave loading of subscale disks and flat plates. Disks and plates were delivered to DRI in a preshock heat treated condition in accordance with processing Schedules I and II.

Flyer plate shocking was selected, as opposed to direct contact shocking, on the basis that this approach yielded larger improvements in both LCF life and tensile properties in the previous program. Property improvements were attributed to a higher dislocation density substructure in the flyer plate versus direct contact shocked material. Figure 6 shows a sketch of the simulated plane wave generator flyer plate apparatus used to shock the disks. The apparatus consisted of twenty detonation cords of the same length set in a pattern of concentric circles attached to layers of Detasheet C-8 explosive. Design of this arrangement promotes uniform detonation of explosive and results in a planar impact of the flyer plate at the disk surface. The entire assembly was supported over a cardboard barrel filled with water such that the disks were quenched immediately after shocking to prevent any thermally induced effects.

Each disk was potted in lead within a circular steel plate prior to shocking. This procedure provides for planar flyer plate impact at the irregular disk surfaces. Potting was accomplished by pouring liquid lead through the 1.6 cm (0.006 in.) diameter potting hole drilled in the bore of each disk.

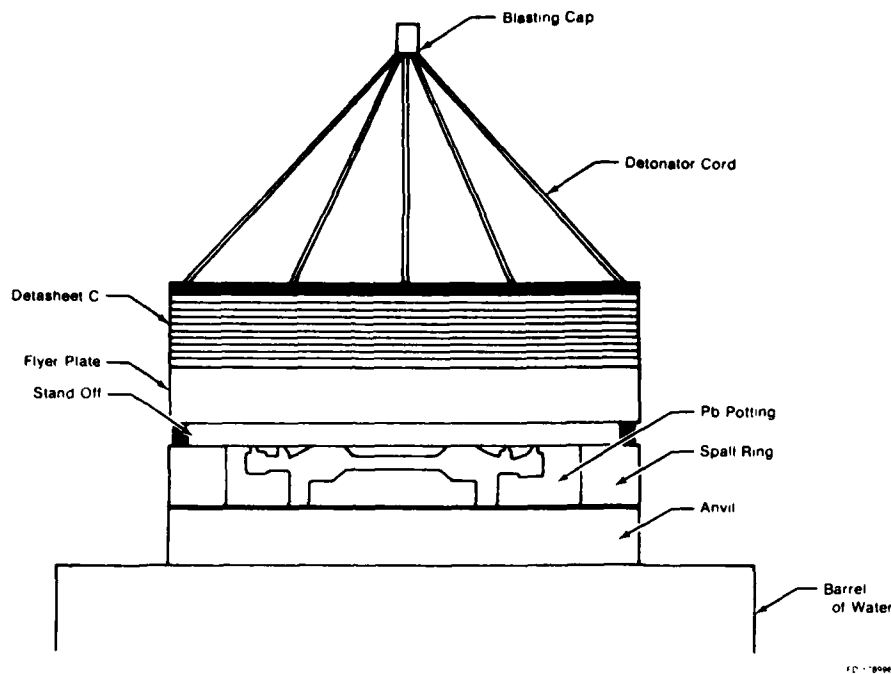


Figure 6. Shock Wave Apparatus, Simulated Plane Wave Generator

Four disks from each processing schedule were used to establish peak pressures in the following manner: Schedule I — one F100B and three TF30 disks; Schedule II — four TF30 disks. In order to eliminate disk type as a variable in establishing peak shocking pressure for the two schedules, peak pressures were established on the TF30 disk type for both schedules. As a starting point, disks were peak pressure shocked at 17,500 MPa (2540 ksi/175 kbar). The remaining three disks in each schedule underwent shocking at decreasing pressures in increments of 2500 MPa (360 ksi/25 kbar). This testing resulted in the establishment of 10,000 MPa (1450 ksi/100 kbar) and 15,000 MPa (2175 ksi/150 kbar) peak pressures on TF30 disks for Schedules I and II, respectively. Table 2 summarizes the disk shocking.

Three flat plates from each processing schedule were shocked at the respective peak pressures established on Schedules I and II TF30 disks. The Schedule I plates were shocked at 10,000 MPa (1450 ksi/100 kbar) and the Schedule II plates were shocked at 15,000 MPa (2175 ksi/150 kbar).

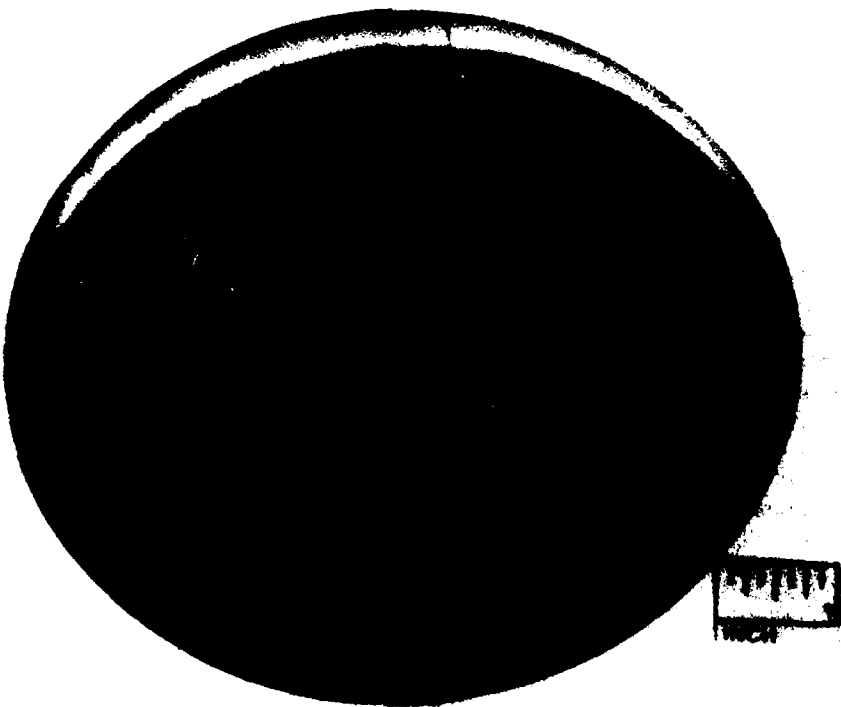
Flat plate No. 1 (Schedule I) underwent shocking at 10,000 MPa (1450 ksi/100 kbar) with the same shocking apparatus used for the disks, as shown in Figure 6. Visual plate inspection following shocking revealed a large radial crack, as shown in Figure 7. In an attempt to prevent cracking of the remaining five plates, the method of explosive detonation was changed from multipoint simulated plane wave to mousetrap plane wave detonation, as shown in Figure 8, to promote uniform explosive detonation and a more planar flyer plate impact. The method was not successful as cracks were still observed in each shocked plate.

TABLE 2. DISK SHOCKING SUMMARY

Disk No	Disk Type	Schedule	Shocking Pressure MPa (ksi) (kbar)	Shocking Effects
1	F100B, 1st stage	I	17,500 (2540) (175)	Disk Fracture
2	TF30, 1st stage	I	15,000 (2175) (150)	Disk Fracture
3	TF30, 1st stage	I	12,500 (1810) (125)	Disk Fracture
4	TF30, 1st stage	I	10,000 (1450) (100)	None
5	F100B, 1st stage	I	Unshocked	
6	TF30, 1st stage	II	17,500 (2540) (175)	Disk Fracture
7	TF30, 1st stage	II	15,000 (2175) (150)	Disk Fracture
8	TF30, 1st stage	II	15,000 (2175) (150)	None
9	TF30, 1st stage	II	15,000 (2175) (150)	Disk Fracture
10	F100, 1st stage	II	Unshocked	

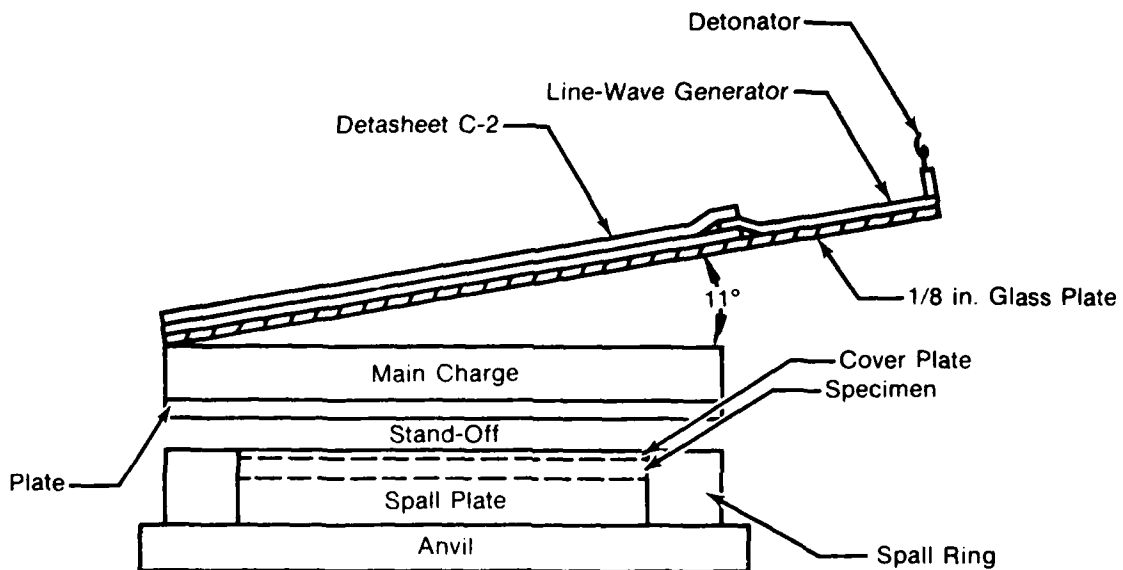
A 10,000 MPa (1450 ksi/100 kbar) peak pressure shock was established on Schedule I processed disks.

A 15,000 MPa (2175 ksi/150 kbar) peak pressure shock was established on Schedule II processed disks.



FAL 58242

Figure 7. Flat Plate No. 1 — Schedule I, Shocked at 10,000 MPa (1450
ksi/100 kbar)



FD 206579

Figure 8. Shock Wave Apparatus, Mousetrap Plane Wave Generator

METALLOGRAPHY

Metallographic examinations were performed on as-extruded billet, disk and flat plate material. A transverse section of as-extruded material was examined prior to processing of the disks and plates. Cross sections through the disk diameter were obtained at each stage of processing Schedules I and II. Flat plates were examined in the as-shocked and final post-shock heat treated condition for each schedule.

Standard polishing procedures were used to prepare metal surfaces of the as-extruded billet and disks for metallographic examination. Grinding through 600-grit silicon carbide paper was followed by mechanical polishing with 6μ and 1μ diamond paste. Specimens were etched with Kalling's and Glyceregia etchants to delineate grain structure and γ' precipitate morphology, respectively.

Microstructures of flat plates were replicated in order to preserve the flat plate material for mechanical testing. Impact and opposite surfaces of plates were polished using an air gun with a sanding disk attachment. Mid-radius locations were polished through 600-grit silicon carbide paper followed by mechanical polishing with 6μ and 1μ diamond paste. Polished surfaces were etched with Kalling's and Glyceregia etchants and coated with acetone. Cellulose tape was placed over the acetone area for replication. After drying, replicas were removed from the plate surface and placed on a glass slide for examination.

Transmission electron microscopy (TEM) studies were performed on peak-pressure shocked and control disks at each stage of processing Schedules I and II. Thin foils were prepared from transverse slices at the center of the disk cross sections. Initial slices of approximately 1.25 mm (0.05 in.) thick were ground on 320-grit silicon carbide paper to 0.380 mm (0.015 in.) and then to 0.125 mm (0.005 in.) on 600-grit silicon carbide paper. Samples of 0.31 mm (0.012 in.) diameter were then punched from the 0.125 mm (0.005 in.) samples for the subsequent thinning operations.

Preparation of electron transparent regions was accomplished with a Fischione Model 110 electropolishing unit used in conjunction with a Model 120 power controller. The electrolyte, 13% H₂SO₄ in methanol, was held between -15 and -10°C (5 and 14°F) and minimum detectable jet flows were utilized during polishing. Current settings varied with each specimen with the range of 40 to 60 ma at 20 vdc.

MECHANICAL TESTING

Mechanical testing on the control and shockwave-processed flat plates of Schedules I and II included low-cycle fatigue (LCF), stress-rupture, tensile, and hardness. The LCF specimens were machined from tangential sections of the flat plates, since the tangential direction is where the maximum stresses operate in turbine disks. Stress-rupture and tensile specimens were machined from random plate locations.

LCF, tensile, and stress-rupture testing was performed in accordance with the PWA 1073 (IN-100) specification. Tests were conducted in air at temperatures which simulated disk operating temperatures. Chromel-alumel thermocouples mounted on the gage section of the test specimens provided temperature monitoring.

Strain-control axial LCF testing was accomplished at 540°C (1000°F) and 650°C (1200°F). Testing involved a cycle strain range of 0 to 1% about a mean strain of 0.5% at a frequency of 0.166 Hz (10 cycles/min). Figure 9 details the test specimen configuration.

Stress-rupture testing was performed in air under constant load. Specimens were loaded to a 640 MPa (92.5 ksi) stress level and tested at 730°C (1350°F). Figure 10 shows the test specimen configuration.

Tensile testing was performed at 705°C (1300°F) using a cross-head speed of 3.70 mm/min. (0.15 in./min.). Figure 11 illustrates the test specimen configuration.

Hardness surveys were made on both control and peak-pressure shocked disks and plates. Disk hardness was evaluated through the maximum thickness and across the diameter at the center of the cross section at each stage of processing. Plate hardness measurements were conducted at the center of the impact and opposite surfaces.

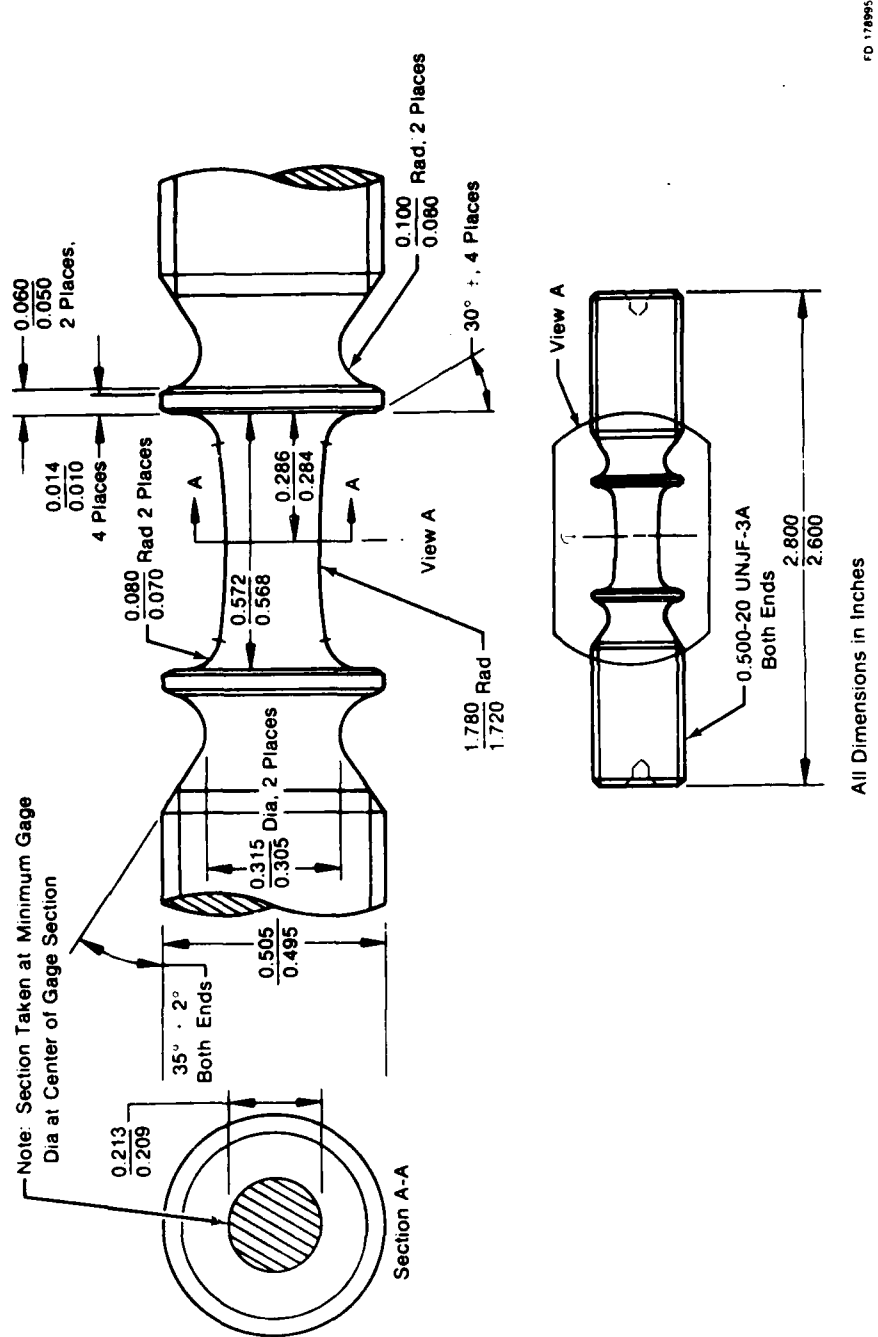
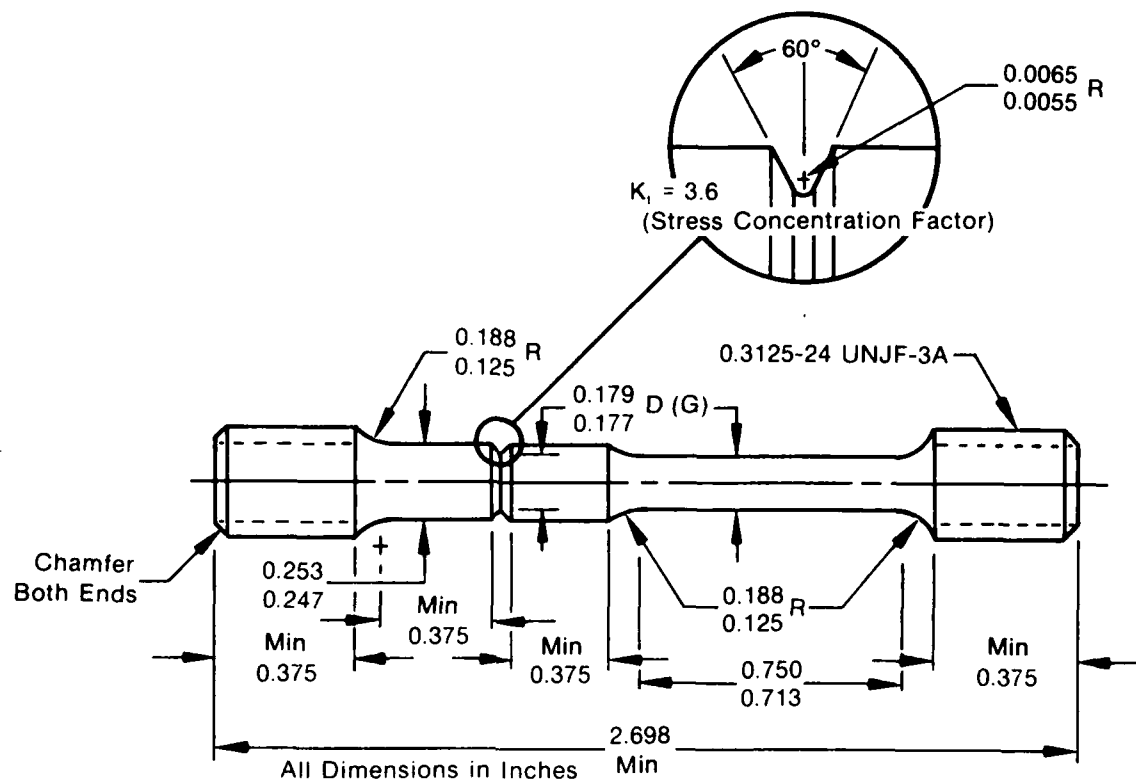
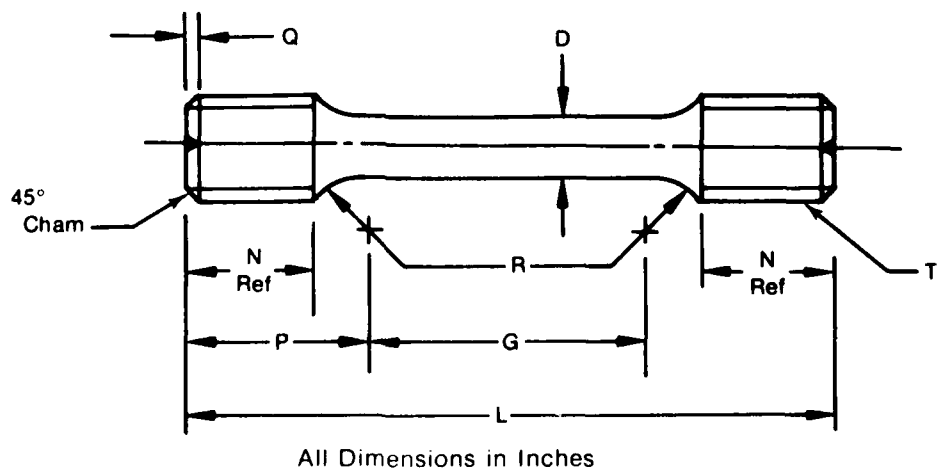


Figure 9. Strain Control Low-Cycle Fatigue Specimen



FD 206541

Figure 10. Combination Stress-Rupture Specimen



± 0.001	D	G	L	N	P	Q	R	T
	0.252	1.062	2.750	0.625	0.844	0.055	0.250	0.500 - 13 UNJC-3A

FD 176994

Figure 11. Standard Round Bar Tensile Specimen

SECTION IV

RESULTS AND DISCUSSION

PEAK-PRESSURE SHOCKING

Testing established peak shocking pressures of 10,000 MPa (1450 ksi/100 kbar) for Schedule I and 15,000 MPa (2175 ksi/150 kbar) for Schedule II sonic-shaped subscale disks. The peak-pressure shocked disks showed no indication of fracture on binocular inspection, although subsequent metallographic examinations revealed fine shallow cracks propagating from the sharp radii of the disk cross sections.

Fracture locations on shocked disks used to establish peak pressures were documented. Generally, cracking appeared more prevalent opposite the flyer plate impact surface. The higher shocking pressures promoted heavy rim damage. Lower pressures resulted in circumferential mid-rim and radial potting hole cracks.

F100B Disks No. 1 (Schedule I) and No. 6 (Schedule II) sustained the most severe damage. These disks were the only F100B-type disks shocked. Shocking at the maximum pressure investigated of 17,500 MPa (2540 ksi/175 kbar) destroyed the entire rim section of both disks as shown in Figures 12 and 13. In addition, cracks were observed in both disks, propagating from the potting holes at the impact and opposite surfaces. The 15,000 MPa (2175 ksi/150 kbar) shocked Disk No. 2 (Schedule I) displayed circumferential mid-rim and radial potting hole cracks opposite the impact surface, as shown in Figure 14, and a small radial potting hole crack at the impact surface. The 15,000 MPa shocked Disk No. 7 (Schedule II) exhibited partial rim removal, as shown in Figure 15. Disk No. 9 showed fractures similar to Disk No. 2, as shown in Figure 16. The 12,500 MPa (1810 ksi/125 kbar) shocked Disk No. 3 (Schedule I) showed a circumferential mid-rim crack opposite the impact surface, as noted in Figure 17.

MECHANICAL TESTING

Control Materials

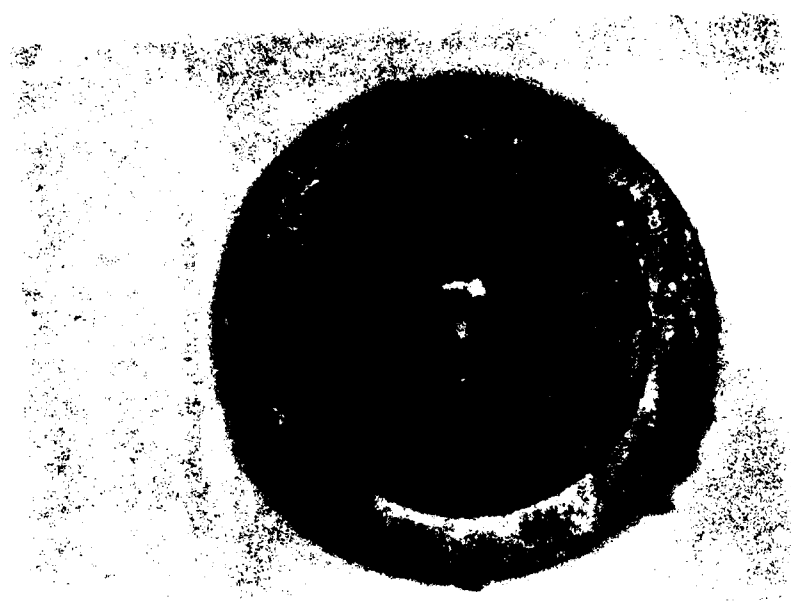
Results of mechanical testing appear in Table 3. A statistical analysis of the data is presented in Table 5.

Mean and two sigma (2σ) lower bound for 540°C (1000°F) and 650°C (1200°F) low-cycle fatigue (LCF) life of Schedules I and II materials significantly exceeded PWA 1073 specification values for full-scale IN-100. This apparent improvement in LCF life resulted from this subscale heat treatment effect commonly observed with IN-100. Traditionally, the IN-100 alloy has been more sensitive to the higher heating and cooling rates experienced in subscale than in fullscale materials. The observed increase in LCF life results from the more efficient quench following the solution cycle, the more rapid air cooling following the aging heat treatments, and the longer effective time at aging temperatures.

Scanning electron microscopy (SEM) examinations revealed no apparent trend in failure origin of LCF specimens. Five of the eight specimens failed at voids. One specimen tested at 540°C (1000°F) from each schedule failed at silica-alumina-magnesia inclusions. Figure 18 shows SEM photographs of typical void and inclusion failures. The fracture origin remained indeterminate in one of the 540°C (1000°F) Schedule II specimens.

Substantial increases resulted for both Schedules I and II in mean 730°C/637.9 MPa (1350°F/92.5 ksi) stress-rupture life relative to the full-scale IN-100 PWA 1073 specification level. As in the case of LCF life, this increase was attributed to the subscale heat treatment effect.

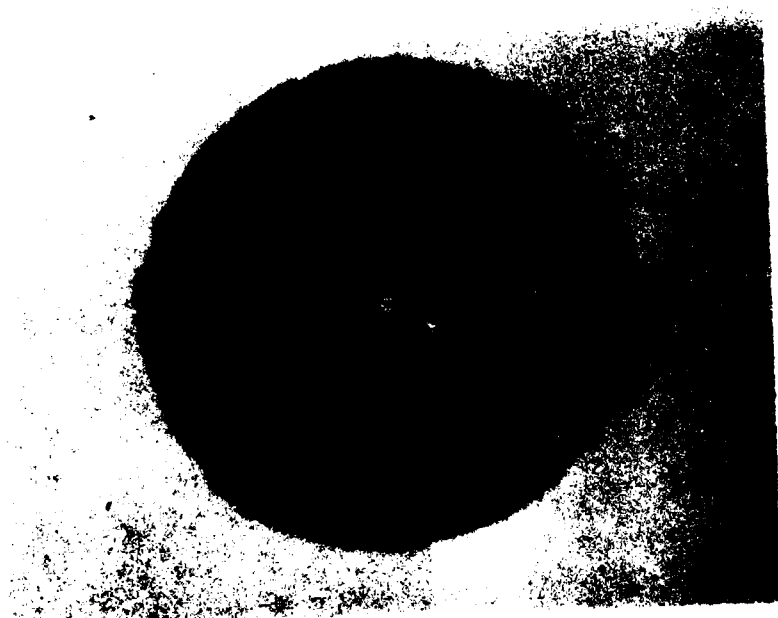




Mag: 0.75X

FAL 58089

(a) Impact Surface



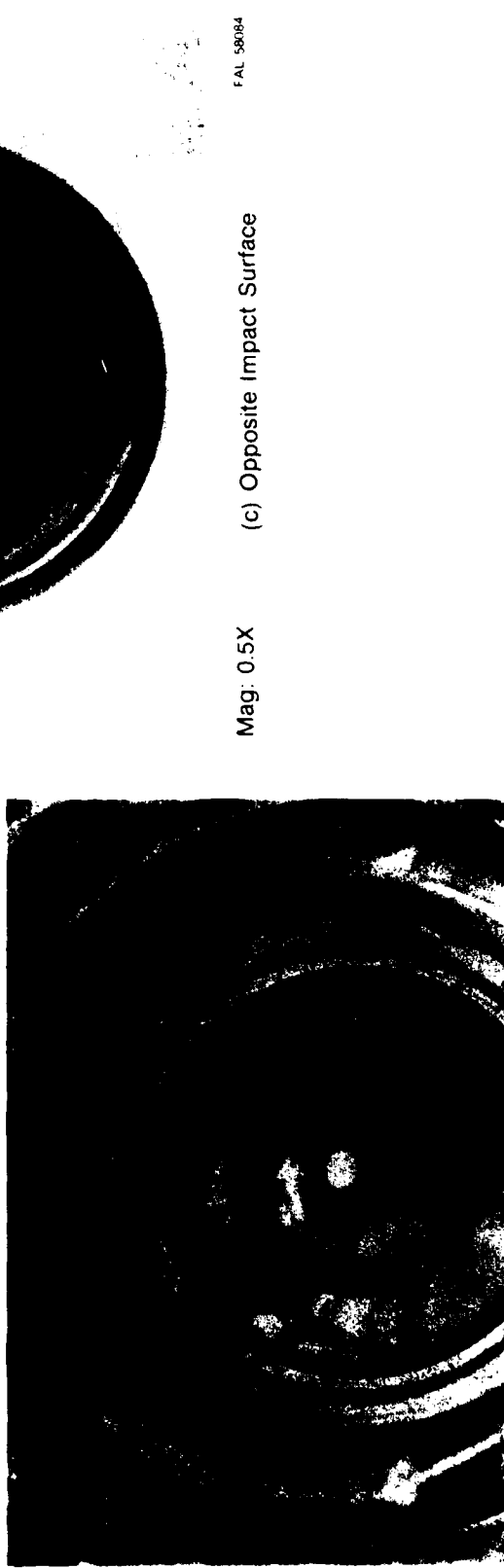
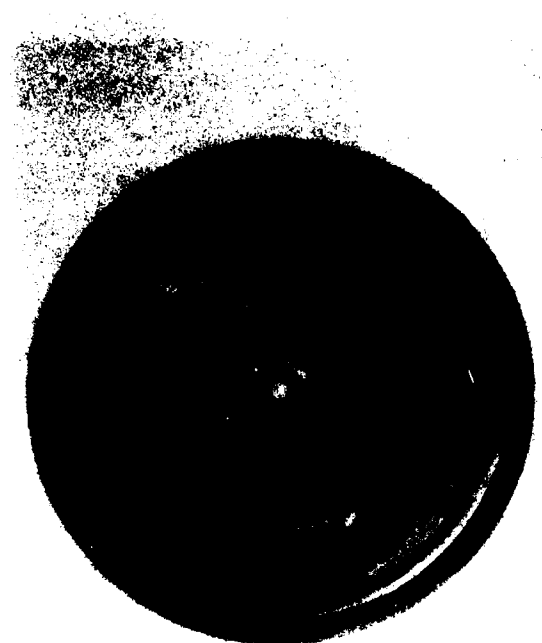
Mag: 0.75X

FAL 58083

(b) Opposite Impact Surface

FD 206581

Figure 13. F100B Subscale Disk No. 6 — Schedule II, Shocked at 17,500 MPa (2540 ksi/175 kbar)



FD 206582

Figure 14. TF30 Subscale Disk No. 2 — Schedule II. Shocked at 15,000 MPa (2175 ksi 150 kbar)



Mag: 0.5X (a) Impact Surface



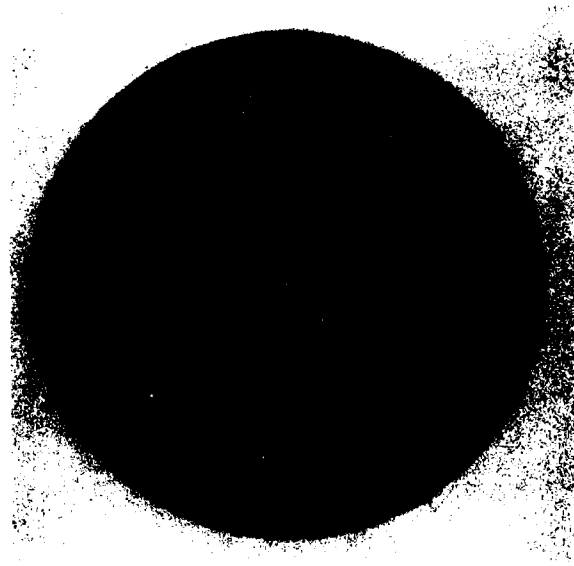
Mag: 0.5X (b) Opposite Impact Surface

FD 181299

Figure 15. TF30 Subscale Disk No. 7 — Schedule II, Shocked at 15,000 MPa (2175 ksi 150 kbar)



Mag: 0.5X (a) Impact Surface



Mag: 0.5X (b) Opposite Impact Surface

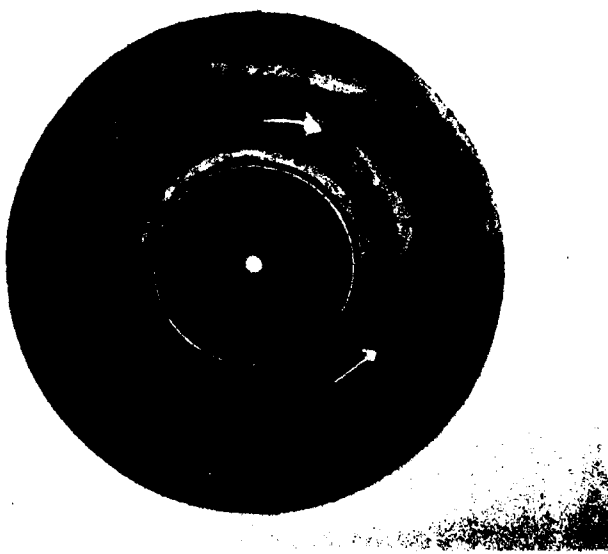
FD 181300

Figure 16. TF30 Subscale Disk No. 9 - Schedule II, Shocked at 15,000 MPa (2175 ksi 150 kbar)



Mag: 0.5X

(a) Impact Surface



Mag: 0.5X

(b) Opposite Impact Surface

FD 210151

Figure 17. TF30 Subscale Disk No. 3 — Schedule I, Shocked at 12,500 MPa (1810 ksi/125 kbar)



Mag: 500X

a.



Mag: 1000X

b.



Mag: 500X

c.

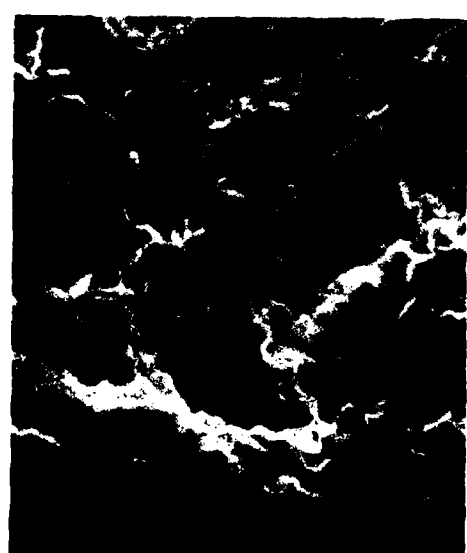
c. and d.

a. and b. Void Failure - Schedule I Control



Mag: 500X

e.



Mag: 1000X

f.

e. and f. Void Failure - Schedule II Control



Mag: 500X

g.

g. and h.

Figure 18. SEM Photographs of Typical Void and Inclusion Low-Cycle Fatigue Fracture



b.



Mag: 500X

c.



Mag: 1000X

d.

c. and d. Inclusion Failure - Schedule I Control

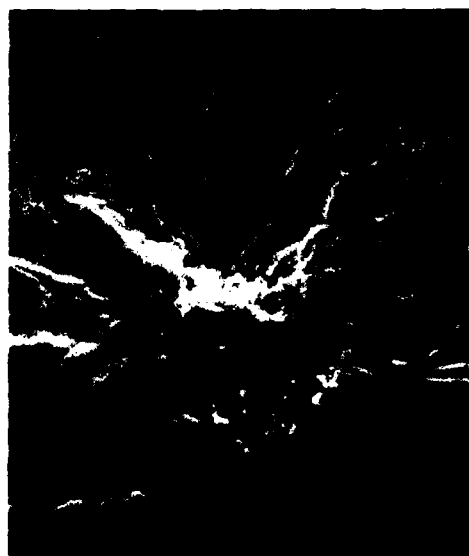


f.



Mag: 500X

g.



Mag: 1000X

h.

g. and h. Inclusion Failure - Schedule II Control

FD 206585

of Typical Void and Inclusion Low-Cycle Fatigue Fracture Origins

TABLE 3. MECHANICAL TESTING RESULTS OF CONTROL MATERIALS

Low-Cycle Fatigue Properties					
Specimen No.	Plate No.	Schedule No.	Failure Cycles	Failure Cycles	
			1000°F (538°C)	1200°F (649°C)	
1	4	I	23902	—	
2	4	I	4102	—	
3	4	I	—	5284	
4	4	I	—	6347	
1	8	II	7921	—	
2	8	II	10417	—	
3	8	II	—	6322	
4	8	II	—	11311	
Stress-Rupture Properties - 730°C 637.9 MPa (1350°F 92.5 ksi)					
Specimen No.	Plate No.	Schedule No.	Stress-Rupture Life (hr)	Elongation (%)	Reduction In Area (%)
1	4	I	79.7	12.7	23.0
2	4	I	85.2	15.9	23.6
3	4	I	84.4	11.9	20.5
1	8	II	53.7	11.1	20.1
2	8	II	51.8	11.8	18.1
3	8	II	48.9	11.5	19.8
Tensile Properties - 705°C (1300°F)					
Specimen No.	Plate No.	Schedule No.	0.2% Offset Yield Strength (MPa) (ksi)	Ultimate Strength (MPa) (ksi)	Elongation (%) Reduction In Area (%)
1	4	I	1089.7	158.0	1267.6 183.8 19.3 20.5
2	4	I	1085.5	157.4	1282.8 186.0 22.0 22.7
1	8	II	1057.2	153.3	1262.1 183.0 26.7 26.6
2	8	II	1085.5	157.4	1244.9 180.5 25.3 29.5
Disk Hardness (R _c)					
Disk No.	Schedule No.	As Preshock Heat Treated (Survey 1)*		As Postshock Heat Treated (Survey 1)*	
5	I	42.2		43.1	
10	II	42.5		42.7	
Plate Hardness (R _c)					
Plate No.	Schedule No.	As Preshock Heat Treated (Survey 3)**		As Postshock Heat Treated (Survey 3)**	
4	I	43.5		45.0	
8	II	44.7		42.9	

*Survey 1 — Average hardness across center of disk cross section.

**Survey 3 — Average hardness at plate center.

Stress-rupture life was significantly longer for Schedule I than Schedule II materials. Mean and 2σ lower bound lives were 38.0 and 31.3% longer, for the Schedule I than Schedule II materials respectively, as a result of the selection of the 870°C (1600°F) and 980°C (1800°F) cycles in the Schedule II heat treatment. These cycles reduce stress-rupture life by coarsening both primary and secondary γ' precipitates. However, they are included in the standard IN-100 PWA 1073 heat treatment (Schedule II) to facilitate final disk machining.

The 705°C (1300°F) tensile properties of the tested specimens from both processing schedules met the full-scale mean IN-100 (PWA 1073) property levels. Schedule I specimens showed slightly higher yield and ultimate tensile strengths, but slightly lower ductility than those of Schedule II, as shown in Tables 3 and 4.

Hardness test results were typical of IN-100, as noted in Table 3. No significant difference existed in hardness level between schedules or individual processing stages.

Shock Wave Processed Materials

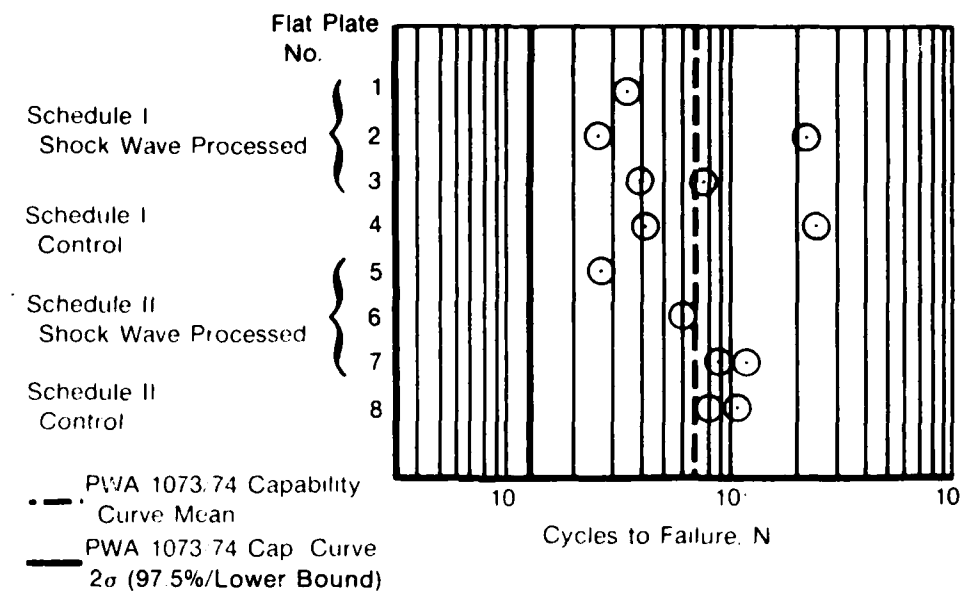
Results of mechanical testing appear in Table 4. A statistical analysis of the data is presented in Table 5.

Low cycle fatigue test results showed no significant improvement of the shocked material in either the 540°C (1000°F) or 650°C (1200°F) life capability relative to the control material. Furthermore, data scatter appeared higher than expected. Graphical presentation of LCF test results is presented in Figure 19.

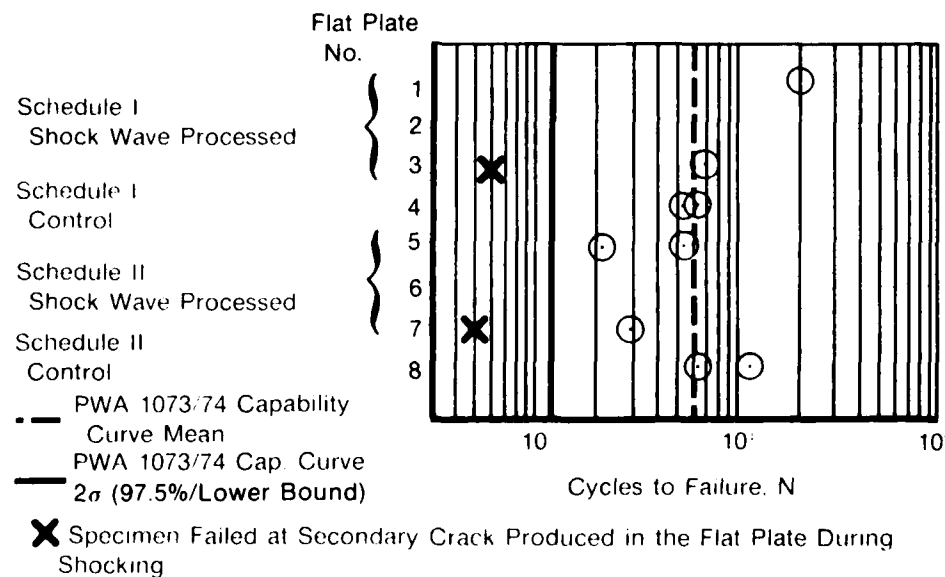
Post-test SEM analyses of six shock wave processed specimens showed fracture origins at silica-alumina-magnesia inclusions, similar to those of control specimens shown in Figure 20, for one specimen from each schedule tested at 540°C (1000°F) and 650°C (1200°F). One specimen from each schedule tested at 650°C (1200°F) failed at secondary cracks produced in the flat plates during shocking, as shown in Figure 20.

Stress-rupture test results indicated no benefit in 730°C 637.9 MPa (1350°F/92.5 ksi) stress-rupture properties due to shock wave processing. In fact, the shock wave processed materials for both processing schedules showed significant reductions in both mean and 2σ lower bound stress-rupture life and ductility relative to control subscale materials.

Mean and 2σ lower bound lives decreased 10.7 and 12.0%, respectively, for Schedule I and 28.7 and 28.6%, respectively, for Schedule II. Mean and 2σ lower bound elongation decreased 29.6 and 47.0, respectively, for Schedule I and 21.9 and 37.3%, respectively, for Schedule II. Of the total of twelve shock treated samples tested from the two schedules, nine initially failed in the notch area of the stress-rupture specimen. In comparison, none of the six control specimens initially failed in the notch section, as noted in Table 3. These results indicate an increase in the notch sensitivity of IN-100 due to shocking.



(a) 540°C (1000°F) Results



(b) 650°C (1200°F) Results

Figure 19. Low-Cycle Fatigue Test Results

TABLE 4. MECHANICAL TESTING RESULTS OF SHOCK WAVE PROCESSED MATERIALS

Low-Cycle Fatigue Properties¹

Specimen No.	Plate No.	Schedule No.	Cycles 1000°F (538°C)	Cycles 1200°F (649°C)
1	1	I	3413	—
2	2	I	2540	—
3	2	I	21560	—
4	3	I	3909	—
5	3	I	7499	—
6	1	I	—	20938
7	2	I	—	9477
8	3	I	—	7013
9	3	I	—	547 ¹
1	5	II	2611	—
2	6	II	5477	—
3	7	II	8746	—
4	7	II	11725	—
5	5	II	—	2067
6	5	II	—	5497
7	7	II	—	477 ¹
8	7	II	—	2925

Stress Rupture Properties - 730°C 637.9 MPa (1350°F 92.5 ksi)

Specimen No.	Plate No.	Schedule No.	Stress-Rupture Life (hr)	Elongation (%)	Reduction In Area (%)
1	1	I	68.6 (33.8 V/N ²)	8.9	16.6
2	1	I	85.2 (65.0 V/N ²)	9.4	13.4
3	1	I	71.4	8.7	14.1
4	2	I	87.9 (61.1 V/N ²)	13.7	16.9
5	2	I	78.7 (61.7 V/N ²)	10.5	17.9
6	3	I	70.8 (32.2 V/N ²)	12.2	14.1
7	3	I	63.6 (37.6 V/N ²)	5.8	10.0
8	3	I	70.5 (52.3 V/N ²)	7.3	13.3
1	5	II	35.6 (18.7 V/N ²)	7.2	6.8
2	7	II	37.8 (24.9 V/N ²)	10.7	13.9
3	7	II	9.8 ¹	—	—
4	7	II	0.2 ¹	—	—

Tensile Properties - 705°C (1300°F)

Specimen No.	Plate No.	Schedule No.	0.2% Offset		Elongation (%)	Reduction In Area (%)		
			Yield Strength (MPa)	Ultimate Strength (MPa)				
1	1	I	1183.4	171.6	1374.5	199.3	16.0	18.5
2	1	I	1186.2	172.0	1348.3	195.5	2.7	5.4
3	2	I	1153.8	167.3	1344.8	195.0	17.3	19.2
4	2	I	1162.1	168.5	1336.6	193.8	17.3	19.7
5	2	I	1149.0	166.6	1356.6	196.7	18.7	22.4
6	3	I	1171.8	169.9	1294.5	187.7	2.7	3.7
7	3	I	1187.6	172.2	1394.5	202.2	6.7	3.7
1	5	II	1228.3	178.1	1364.1	197.8	17.3	21.1
2	5	II	1198.6	173.8	1376.6	199.6	20.0	24.3
3	5	II	1189.0	172.4	1362.1	197.5	17.3	22.4
4	6	II	1186.9	172.1	1362.1	197.5	14.7	12.9
5	6	II	1179.3	171.0	1374.5	199.3	17.3	21.6
6	6	II	1166.2	169.1	1366.9	198.2	16.0	19.2
7	7	II	1147.7	166.7	1334.5	193.5	20.0	29.0
8	7	II	1158.6	168.0	1327.6	192.5	5.3	2.3

TABLE 4. MECHANICAL TESTING RESULTS OF SHOCK WAVE PROCESSED MATERIALS (Continued)

Disk Hardness (R_c)							
Disk	Schedule No.	As-Preshock Heat Treated		As-Shocked		As-Postshock Heat Treated	
		(Survey 1)*	(Survey 1)	(Survey 2)**	(Survey 1)*	(Survey 2)**	
4	I	42.2	47.4	1. 45.8	47.5	1. 47.5	
				2. 47.4		2. 47.4	
				3. 46.2		3. 47.0	
				4. 47.0		4. 46.6	
				5. 45.3		5. 47.6	
8	II	42.3	47.9	1. 51.1	47.0	1. 47.5	
				2. 48.2		2. 47.4	
				3. 47.6		3. 47.0	
				4. 48.2		4. 47.3	
				5. 46.4		5. 45.9	

Plate Hardness (R_c) -- Survey 3***							
Plate No.	Schedule No.	As-Preshock Heat Treated		As-Shocked		As-Postshock Heat Treated	
		Impact Surface	Opposite Surface	Impact Surface	Opposite Surface	Impact Surface	Opposite Surface
1	I	43.5	43.3	46.5	42.7	46.0	
2	I	43.5	45.3	46.0	45.1	45.1	
3	I	43.5	44.4	46.2	44.2	43.4	
5	II	44.7	48.6	48.5	46.8	47.6	
6	II	44.7	43.7	49.2	43.9	45.1	
7	II	44.7	47.3	48.1	45.3	46.3	

Specimen failed at secondary crack produced in the flat plate during shocking. Value was excluded from the data.
V/N -- Stress-rupture specimen initially failed at the V-notch. Specimen was retested to failure in smooth gage section.

*Survey 1 — Average hardness across center of disk cross sections.

**Survey 2 — Hardness through maximum thickness areas of peak pressure shocked disk cross sections-impact surface (1) to opposite surface (5).

***Survey 3 — Average hardness at plate center.

TABLE 5. MECHANICAL PROPERTIES — STATISTICAL ANALYSIS

Low-Cycle Fatigue Properties						
Material	Cycle to Failure 538°C (1000°F)			Cycles to Failure 650°C (1200°F)		
	Mean	2 σ Lower Bound	Mean	2 σ Lower Bound		
Full-Scale IN-100 PWA 1073	4550	910	3000	560		
Controls Schedule I	9901	2286	5791	1337		
Shock Wave Processed Schedule I	5594	1291	11164	2577		
Controls Schedule II	9083	2097	8456	1952		
Shock Wave Processed Schedule II	6188	1428	3215	742		
Stress-Rupture Properties - 730°C 637.9 MPa (1350°F 92.5 ksi)						
Material	Life (hr)		Elongation (%)		Reduction In Area (%)	
	Mean	2 σ Lower Bound	Mean	2 σ Lower Bound	Mean	2 σ Lower Bound
Full-Scale IN-100 PWA 1073	32.0	—	—	—	—	—
Controls Schedule I	83.0	64.7	13.5	6.6	22.3	15.7
Shock Wave Processed Schedule I	74.1	56.9	9.5	3.5	14.5	8.5
Controls Schedule II	51.4	44.4	11.4	6.7	19.3	9.6
Shock Wave Processed Schedule II	36.6	31.7	8.9	4.2	10.3	0.6
Tensile Properties - 705°C (1300°F)						
Material	Yield Strength 0.2% Offset ($\frac{\text{MPa}}{\text{ksi}}$)		Ultimate Tensile Strength ($\frac{\text{MPa}}{\text{ksi}}$)		Elongation (%)	
	Mean	2 σ Lower Bound	Mean	2 σ Lower Bound	Mean	2 σ Lower Bound
Full-Scale IN-100 PWA 1073	1089.7 158.0	—	1255.2 182.0	—	18.0	—
Controls Schedule I	1087.6 157.7	1041.4 151.0	1275.2 184.9	1240.0 179.8	20.6	9.6
Shock Wave Processed Schedule I	1166.9 169.2	1120.7 162.5	1351.7 196.0	1316.6 190.9	14.4	3.4
Controls Schedule II	1071.0 155.3	1024.9 148.6	1253.1 181.7	1217.9 176.6	26.0	15.0
Shock Wave Processed Schedule II	1182.4 171.4	1135.9 164.7	1357.9 196.9	1322.8 191.8	15.9	4.9
					19.1	3.5



Mag: 200X

(a) Schedule I
10.000 MPa (1450 ksi/100 kbar) Shock



Mag: 200X

(b) Schedule II
15.000 MPa (2175 ksi/150 kbar) Shock

FD 206586

Figure 20. SEM Photographs — Low-Cycle Fatigue Fracture Origins at Shock Wave Induced Secondary Cracks

Tensile test results showed shock processing afforded only a small increase in IN-100 705°C (1300°F) strength, although a substantial reduction in ductility was observed. Strength improvement was attributed to the complex dislocation substructure created by shocking. Shock processing increased mean yield and ultimate tensile strengths between 6 and 10%, while mean elongation decreased between 30 and 80%.

Hardness test results indicated hardness increases for Schedule I and Schedule II processed materials over their respective subscale control materials. No significant hardness difference existed between the two processing schedules. For both schedules, average hardness increases generally ranged between 1 and 5 points on the Rockwell C scale between the pre-shocked and as-shocked states. Increases were observed through the entire thickness of the plates and disks for both schedules. The postshock heat treatments were observed to reduce hardness gradients with little effect on the level of as-shocked hardness.

MICROSTRUCTURAL EXAMINATIONS

Optical microscopy examinations were performed on the as-extruded IN-100 billet and both the control and shock wave processed disks and plates. Representative photomicrographs appear in Figures 21 through 27.

The as-extruded billet microstructure was fully recrystallized, fine grained, and heavily precipitated with γ' . Grain size was predominantly ASTM 14.5. Control and peak-pressure shocked disks displayed typical IN-100 microstructures throughout processing Schedules I and II. Grain size was predominantly ASTM 12.5 in all stages of processing. The γ' morphology and size appeared essentially unchanged. As-shocked and postshock heat treated plates produced the same microstructures.

Surface cracking was observed in both Schedule I and Schedule II peak-pressure shocked disks. Examination of unetched disk cross sections revealed flyer plate impact cracks initiating at sharp radii in the disk cross sections, as shown in Figure 28. Maximum depth of crack propagation was 0.20 cm (0.08 in.).

Transmission electron microscopy (TEM) examinations were accomplished on Schedules I and II control and peak-pressure shocked disks at each stage of processing to observe more subtle microstructural differences and dislocation substructures. Processing effects on size of primary and secondary cooling γ' , carbide type, size and distribution, and dislocation structure appear in Tables 6, 7, and 8, respectively. Representative photomicrographs appear in Figures 29 through 32.

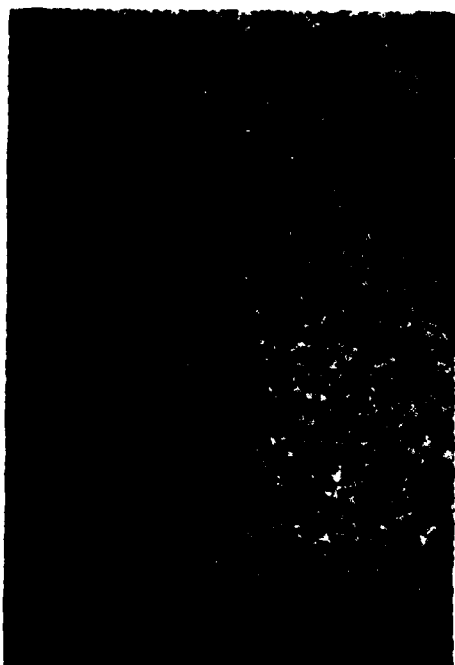
Table 6 summarizes the γ' size distribution observed in disks of Schedules I and II. Examinations of control disks indicated the 870°C (1600°F) + 980°C (1800°F) heat treatment coarsens both primary and secondary cooling γ' , while the 650°C (1200°F) + 760°C (1400°F) cycle ripens only secondary cooling γ' . Shocked disk microscopy revealed the shocking stage prevents any increase in primary cooling γ' size due to the 650°C (1200°F) + 760°C (1400°F) cycle, although there appeared to be no influence of shocking on γ' coarsening in the 870°C (1600°F) + 980°C (1800°F) heat treatment.



Mag: 500 \times Glyceregia Etchant



Glyceregia Etchant Mag: 1000X



Kallings Etchant Mag: 500X



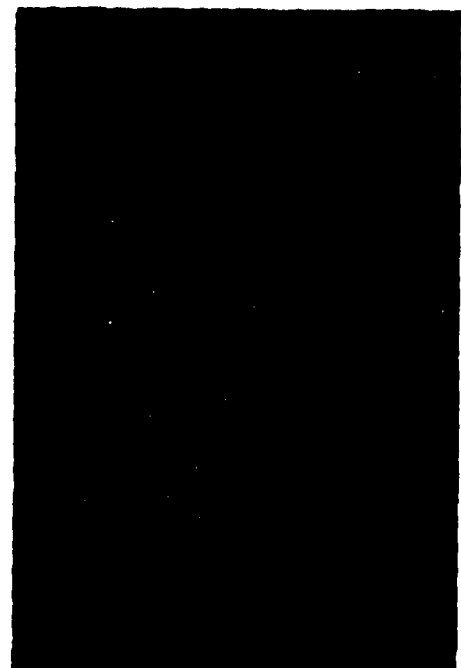
Mag: 1000X **Kalling's Etchant**

Figure 21. As-Extruded IN-100 Billet Microstructure

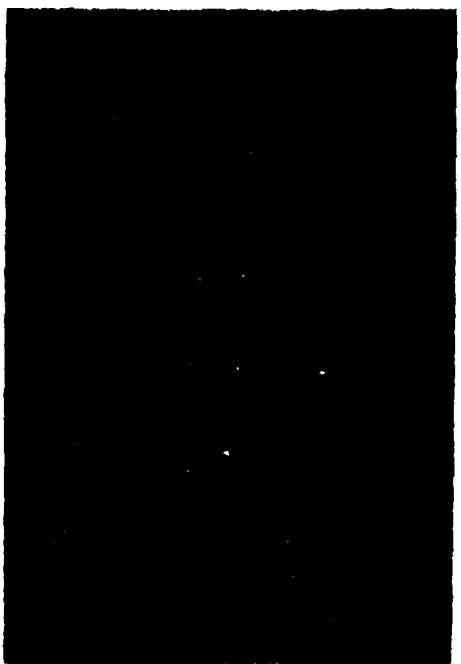
F0 181280



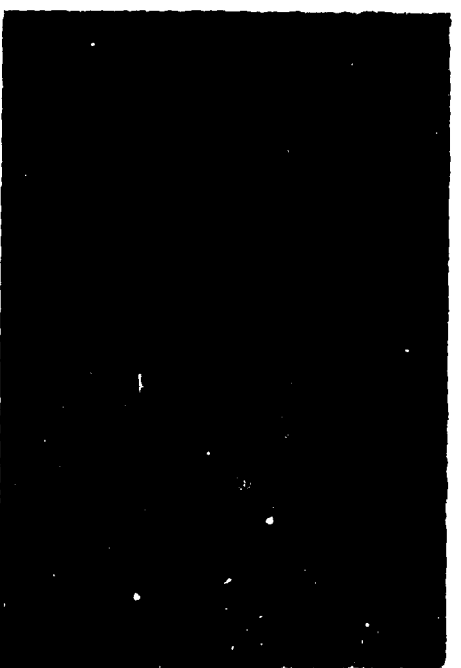
Mag: 500X
Kalling's Etchant
(a) Disk No. 5, Schedule I - Control Disk



Mag: 500X
Kalling's Etchant
(c) Disk No. 10, Schedule II - Control Disk



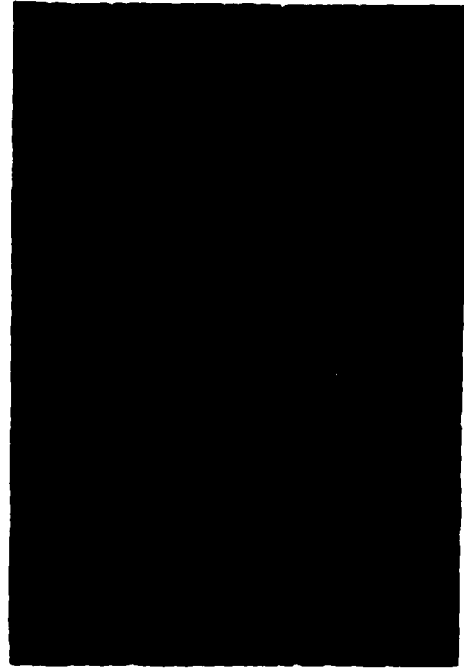
Mag: 500X
Glyceregia Etchant
(b) Disk No. 5, Schedule I - Control Disk



Mag: 500X
Glyceregia Etchant
(d) Disk No. 10, Schedule II - Control Disk

FD 181281

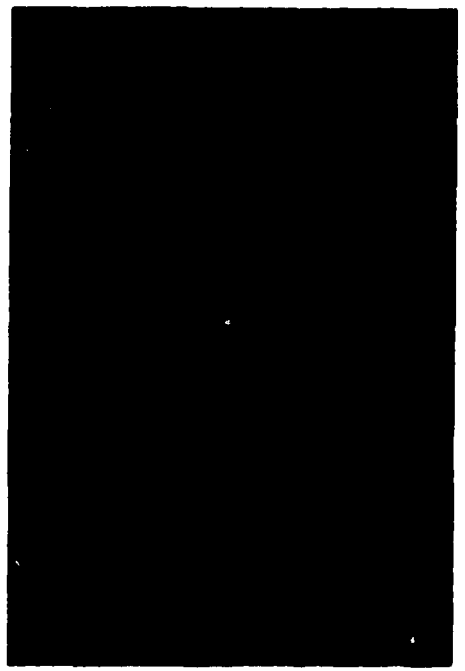
Figure 22. Preshock Heat Treated Disk Microstructures



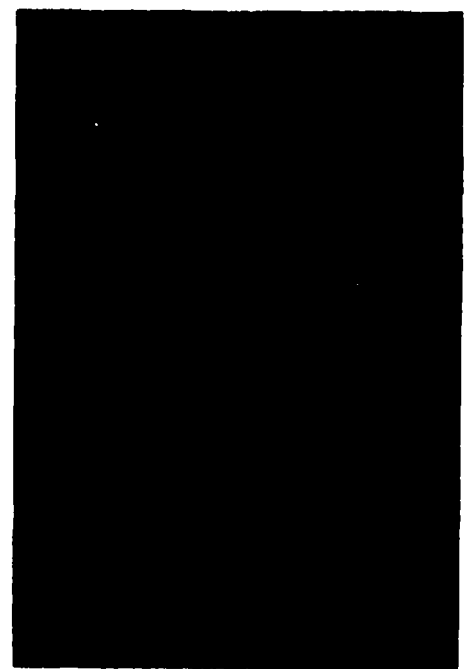
Mag: 500X (a) Disk No. 4 Kalling's Etchant
Schedule I - 10.000 MPa (1450 ksi/100 kbar) Shock



Mag: 500X (b) Disk No. 4
Schedule I - 10,000 MPa (1450 ksi/100 kbar) Shock Glyceregia Etchant



Mag: 500X (c) Disk No. 8
Schedule II - 15,000 MPa (2175 ksi/150 kbar) Shock
Kalling's Etchant



Mag: 500X (d) Disk No. 8 Glyceregia Etchant Schedule II - 15,000 MPa (2175 ksi/150 kbar) Shock

Figure 23 A: Standard West Michigan



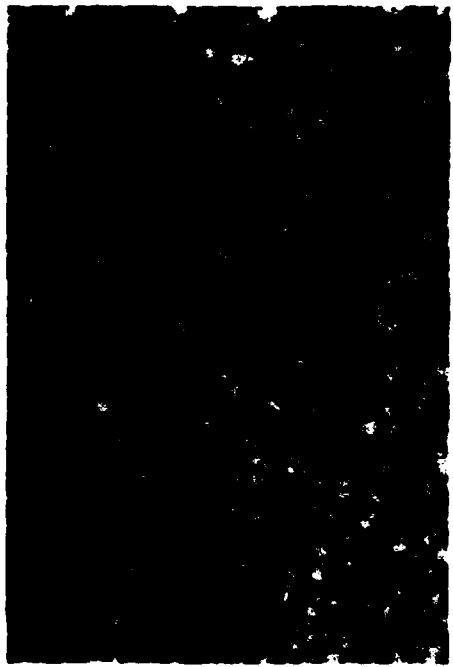
Mag: 500X (a) Disk No. 5, Schedule 1 Kalling's Etchant



Mag: 500X (b) Disk No. 5, Schedule 1 Glyceregia Etchant



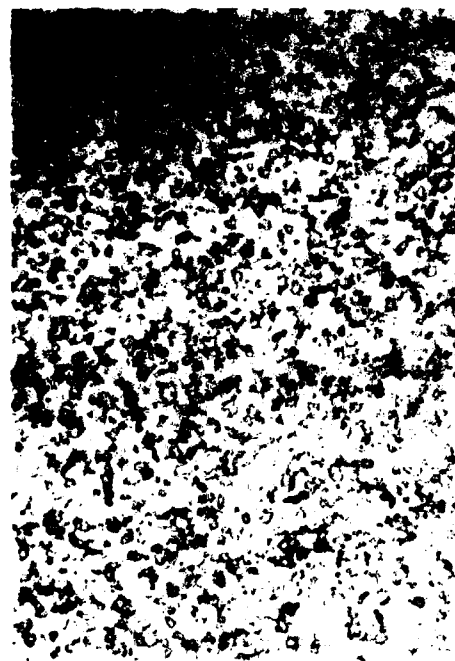
Mag: 500X Glyceregia Etchant (d) Disk No. 10, Schedule 11



Mag: 500X (c) Disk No 10 Schedule II Kalling's Etchant

50 181287

Figure 24. Postshock Heat Treated Disk Microstructures - Control Disks



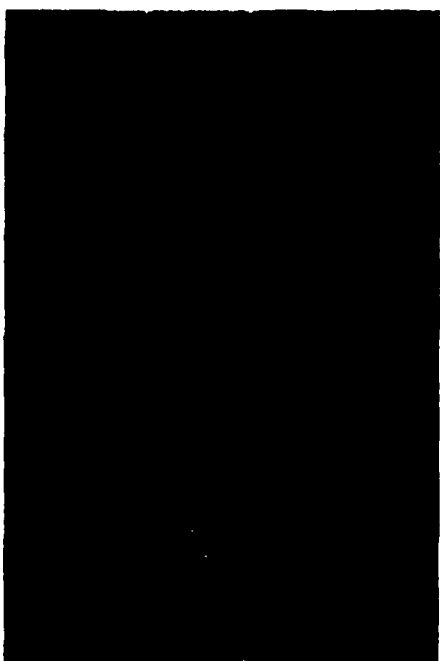
Mag: 500X
Kalling's Etchant
(a) Disk No. 4
Schedule I - 10,000 MPa (1450 ksi/100 kbar) Shock



Mag: 500X
Glyceregia Etchant
(b) Disk No. 4
Schedule I - 10,000 MPa (1450 ksi/100 kbar) Shock



Mag: 500X
Kalling's Etchant
(c) Disk No. 8
Schedule II - 15,000 MPa (2175 ksi/150 kbar) Shock



Mag: 500X
Glyceregia Etchant
(d) Disk No. 8
Schedule II - 15,000 MPa (2175 ksi/150 kbar) Shock

Figure 25. Postshock Heat Treated Disk Microstructures

FD 18-284



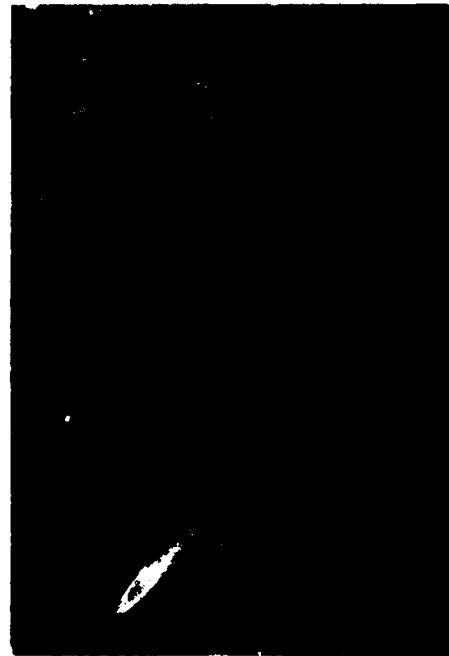
Mag: 500X
Kalling's Etchant
(a) Plate No. 2
Schedule I - 10,000 MPa (1450 ksi/100 kbar) Shock



Mag: 500X
Glyceregia Etchant
(b) Plate No. 2
Schedule I - 10,000 MPa (1450 ksi/100 kbar) Shock

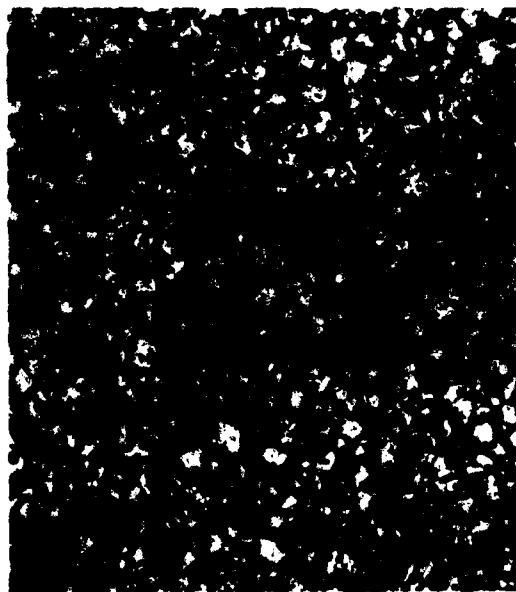


Mag: 500X
Kalling's Etchant
(c) Plate No. 7
Schedule II - 15,000 MPa (2175 ksi/150 kbar) Shock



Mag: 500X
Glyceregia Etchant
(d) Plate No. 7
Schedule II - 15,000 MPa (2175 ksi/150 kbar) Shock

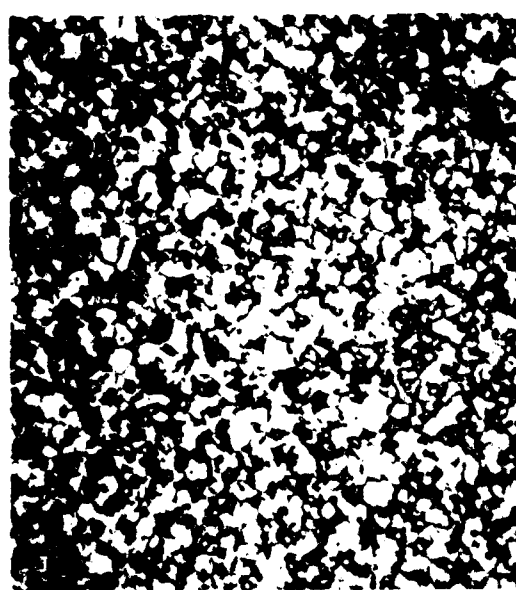
Figure 26. As-Shocked Flat Plate Microstructures



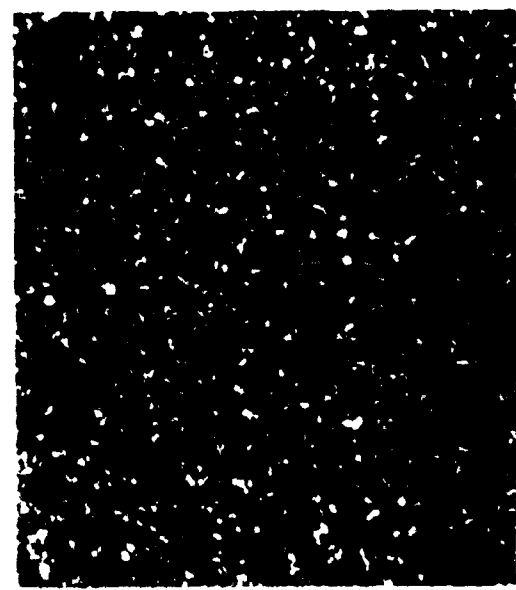
Mag: 500X Kalling's Etchant
(a) Plate No. 2, Schedule I
10,000 MPa (1450 ksi/100 kbar) Shock



Mag. 500X Glyceregia Etchant
(b) Plate No. 2. Schedule I
10,000 MPa (1450 ksi/100 kbar) Shock



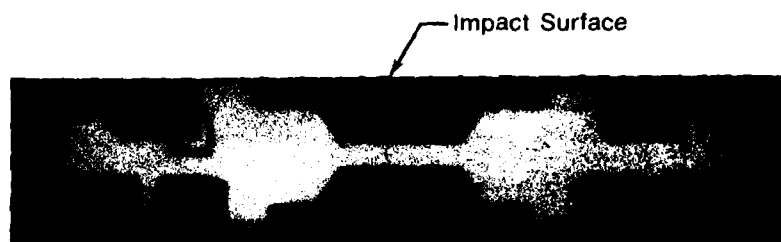
Mag: 500X Kalling's Etchant
(c) Plate No 7, Schedule II
15.000 MPa (2175 ksi/150 kbar) Shock



Mag: 500X Glyceregia Etchant
(d) Plate No 7. Schedule II
15.000 MPa (2175 ksi: 150 kbar) Shock

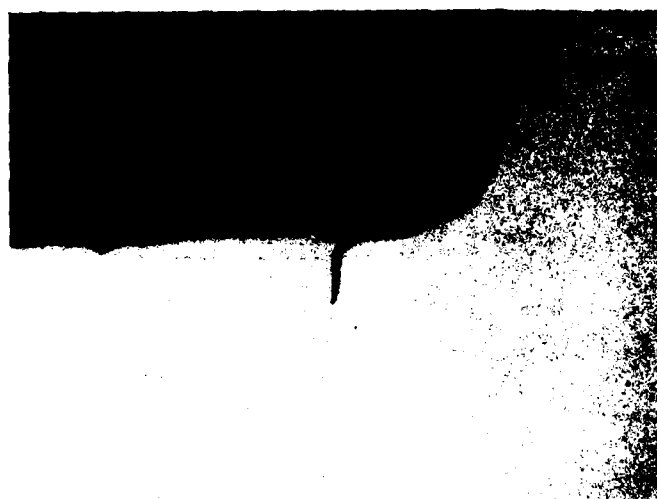
Figure 27. Postshocked Heat Treated Flat Plate Microstructures

10.210162



Mag: 0.67X

(a) TF30 Disk Cross Section, Location
of Impact Surface Crack



Mag: 20X

Unetched

(b) Impact Surface Crack

FD 197975

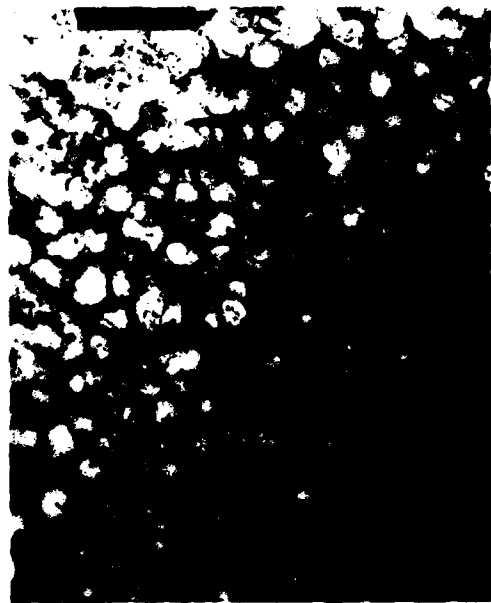
Figure 28. Disk No. 8, Schedule II, Typical Impact Surface Crack

TABLE 6. HEAT TREATMENTS AND MICROSTRUCTURE

Sample	Schedule No.	Post Solution Heat Treatment	Primary Cooling Gamma Prime (nm)	Secondary Cooling Gamma Prime (nm)	Carbide Type
5A	I	None	90-110	7-14	MC
4A	I	10,000 MPa (1450 ksi/100 kbar) Shock	70-150	4-9	MC
5C	I	650 \pm 8°C/24 hr/air cool + 760 \pm 8°C/4 hr/air cool	120-180	10-30	MC
4C	I	10,000 MPa (1450 ksi/100 kbar) Shock + 650 \pm 8°C/24 hr/air cool + 160 \pm 8°C/4 hr/air cool	70-90	10-20	—
10A	II	870 \pm 8°C/40 \pm 5 min/air cool + 980 \pm 8°C/45 \pm 5 min/air cool	100-150	7-15	M ₂₃ C ₆
8A	II	870 \pm 8°C/40 \pm 5 min/air cool + 980 \pm 8°C/45 \pm 5 min/air cool + 15,000 MPa (2175 ksi/150 kbar) Shock	90-180	2-6	MC, M ₂₃ C ₆
10C	II	870 \pm 8°C/40 \pm 5 min + 980 \pm 8°C/45 \pm 5 min + 650 \pm 8°C/24 hr/air cool + 760 \pm 8°C/4 hr/air cool	110-220	4-11	MC
8C	II	870 \pm 8°C/40 \pm 5 min + 980 \pm 8°C/45 \pm 5 min/air cool + 15,000 MPa (2175 ksi/150 kbar) Shock + 650 \pm 8°C/24 hr/air cool + 760 \pm 8°C/4 hr/air cool	90-240	10-20	M ₂₃ C ₆



Mag: 10,500X a



Mag: 48,000X b.



Mag: 22,000X c.



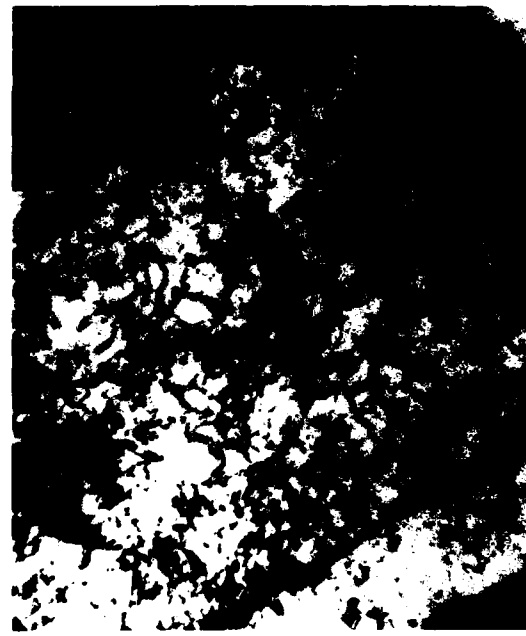
Mag: 48,000X d.

1100146

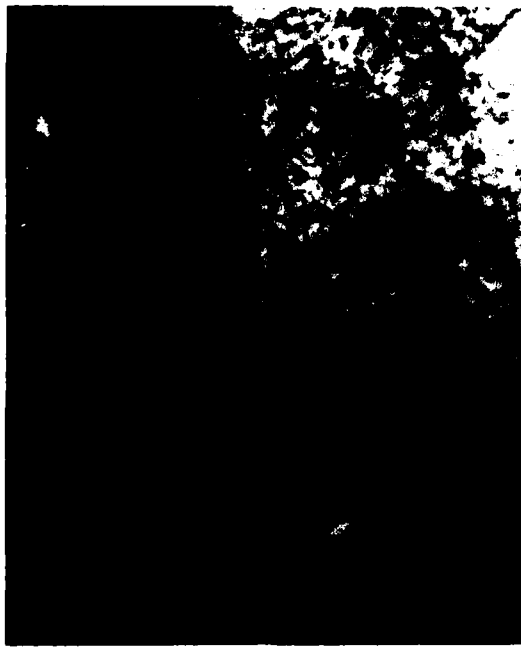
Figure 29. Preshock Heat Treated Disk — Schedule 1



Mag: 10.500X a.



Mag: 22.000X b.



Mag: 22.000X c.



Mag: 48.000X d.

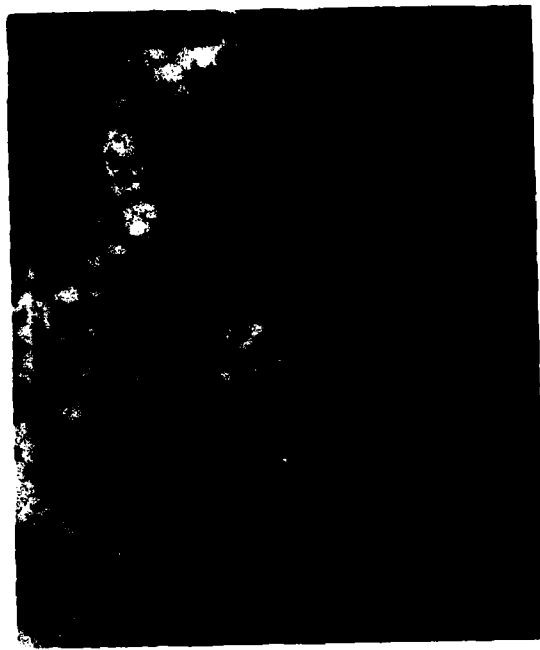
ED 20744

Figure 30. Postshock Heat Treated Disk — Schedule I



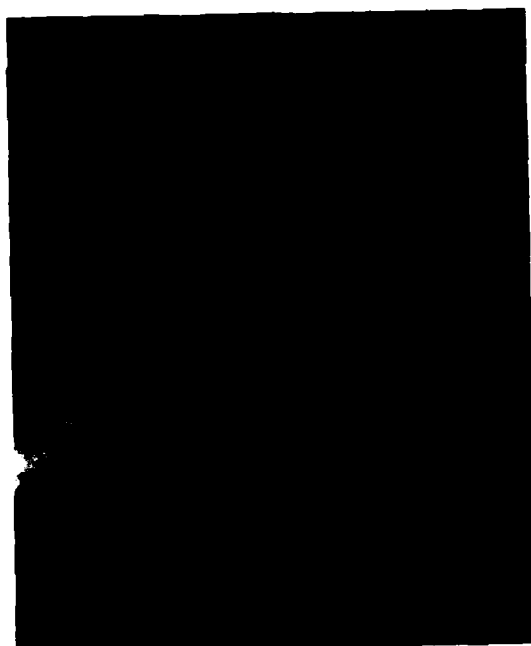
Mag: 4800X

a.



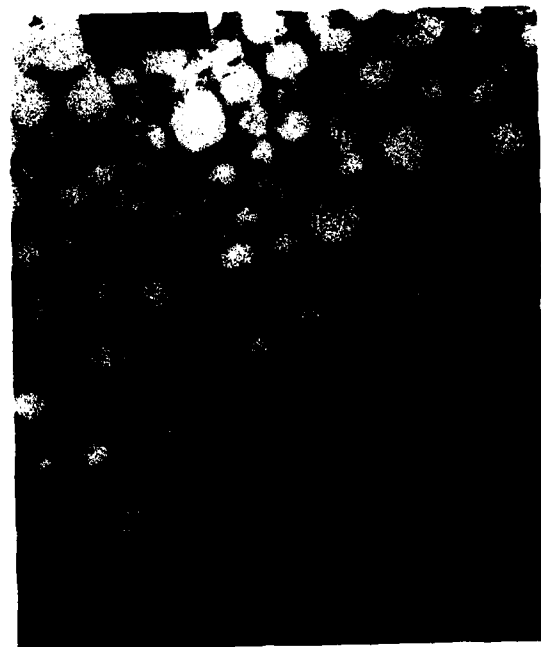
Mag: 22,000X

b.



Mag: 48,000X

c.



Mag: 48,000X

d.

ED 207348

Figure 31. Preshock Heat Treated Disk — Schedule II



Mag: 10,500X a.



Mag: 105,000X b.



Mag: 22,000X c.



Mag: 48,000X d.

FD 207352

Figure 32. Postshock Heat Treated Disk — Schedule II

The dislocation density and structure of the peak-pressure shocked disks during Schedules I and II appear in Table 7. In both schedules, as expected, dislocation density was highest in samples in the as-shocked state. A higher density was observed in Schedule II than in Schedule I, since these disks were shocked at the higher peak pressure. Postshock heat treatment affected dislocation structure in both schedules. Some evidence exists of recovery mechanisms occurring during postshock heat treatment, although no real cellular substructure was observed. Dislocations appeared more uniformly distributed, longer, and more curved in the postshock heat treated samples than in the planar array or band arrangements of the as-shocked state.

Table 8 shows the carbide size distribution noted throughout Schedules I and II. No obvious trends were noted in regard to carbide type, size, or distribution.

TABLE 7. DISLOCATION STRUCTURE

Sample	Schedule No.	Density	Structure
5A	I	Low, mostly in boundaries	Prominent in primary γ' , also in boundaries between grains or between primary γ' regions and $\gamma\text{-}\gamma'$ regions within a grain looped around cooling γ' in matrix.
4A	I	High, somewhat concentrated in boundaries, but no apparent pile-up.	Appear to lie in planar arrays on slip planes Dislocations relatively short and straight.
5C	I	Very low	Similar to 5A
4C	I	High, similar to 4A	No evidence of arrays. Compared to 4A, more in matrix, fewer in primary γ' . Dislocations are longer, multiply curved (winding).
10A	II	Low-moderate, similar to 5A. Some pile-up at boundaries.	Dislocations lie in bands suggestive of fatigue (broken diamond saw blade suspected during specimen preparation). Stacking faults observed.
8A	II	Very high (highest of samples)	Dislocations lie in planes or bands. Generally longer than in 4A, slightly more curved.
10C	II	Low, similar to 5A	Similar to 5A.
8C	II	High	Uniform, dislocations not in planes or bands. Dislocations are shorter, straighter, denser, and less clearly defined than in 4C.

TABLE 8. CARBIDE SIZE AND DISTRIBUTION

Sample	Schedule No.	Size (nm)	Distribution
5A	I	50-500	Uniform. Not many in grain boundaries. Present within both γ' and $\gamma\text{-}\gamma'$ grains.
4A	I	100-400	Uniform. Apparently fewer than in 5A. Small carbides perhaps obscured.
5C	I	30-360	Uniform. Present in γ' and $\gamma\text{-}\gamma'$ grains.
4C	I	180-350	Uniform. Similar to 5C. Small carbides perhaps obscured.
10A	II	50-500	Mostly in grain boundaries. Some in γ' and $\gamma\text{-}\gamma'$ grains.
8A	II	40-600	Similar to 10A, both MC and $M_2\text{C}_6$ in grain boundaries.
10C	II	20-400	Uniform. Many in γ' and $\gamma\text{-}\gamma'$ grains.
8C	II	300-460	Uncertain due to few low magnification pictures. Present in both grain boundaries and matrix.

SECTION V

CONCLUSIONS

1. Peak shock wave working pressures were determined on IN-100 subscale, sonic shaped turbine disks. Pressures of 10,000 MPa (1450 ksi/100 kbar) and 15,000 MPa (2175 ksi/150 kbar) were established for TMP Schedules I and II, respectively.
2. Rim and potting hole areas proved to be the disk locations most susceptible to fracture during shock loading.
3. There was no significant increase in LCF capability of shock wave processed IN-100 at the pressure levels used. LCF improvements cited for shock wave processed materials in References 6, 8, and 9 appear due to the higher shocking pressures employed (50,000 to 53,000 MPa/500 to 527 kbars).
4. Stress-rupture test results show a significant decrease in IN-100 730°C/637.9 MPa (1350°F 92.5 ksi) stress rupture life and ductility. Shocking appears to increase the notch sensitivity of IN-100.
5. Tensile test results indicate only minor improvements in 705°C (1300°F) IN-100 yield and ultimate strengths. Strength increases are accompanied by a substantial reduction in ductility.
6. Peak-pressure shocking affords a hardness increase between 1 and 5 points R_u throughout the subscale disks. Postshock heat treatments reduce hardness gradients with little effect on the level of as-shocked hardness.
7. Shocking appears to prevent ripening of primary cooling γ' during subsequent postshock heat treatment. Dislocation substructures generated by shocking experience limited thermal recovery during postshock heat treatment.

REFERENCES

1. Nolan, M., H. Gadberry, J. Loser, and E. Sneegas, "Explosive Metalworking," High-Velocity Metalworking -- A Survey, NASA Special Publication 5062, NASA Washington, pp. 123-127, 1967.
2. Appleton, A. S., and J. S. Waddington, Phil. Mag., Vol. 12, p. 273, 1965.
3. Peitteiger, L. A., "Explosive Hardening of Nickel Maraging and Manganese Steels," U.S. Naval Weapons Laboratory, Report No. 1934, September 1964.
4. Peitteiger, L. A., "Explosive Hardening of Iron and Low Carbon Steel," U.S. Naval Weapons Laboratory, Report No. 1950, October 1964.
5. Mahajan, S., "Metallurgical Effects of Planar Shock Waves in Metals," Phy. Stat. Sol., Vol. 2, p. 198, 1970.
6. "Thermomechanical Processing of Nickel-Base Superalloys by Shock Wave Deformation," University of Denver, Denver Research Institute Final Technical Report, Contract N00019-72-C-0138, to Naval Air Systems Command, March 1973.
7. Friedel, J., "Dislocations," Pergamon Press, Oxford, p. 187, 1964.
8. "Thermomechanical Processing of Nickel-Base Alloy AF2-1DA Using Shock Wave Deformation," University of Denver, Denver Research Institute Final Technical Report, Contract N00019-74-C-0281, to Naval Air Systems Command, June 1979.
9. "Response of Nickel-Base Superalloys to Thermomechanical Processing by Shock Wave Deformation," University of Denver, Denver Research Institute Final Technical Report, Contract N00019-73-C-0376, to Naval Air Systems Command, April 1974.
10. Robertson, J. M., J. W. Simon, and T. D. Tillman, "Shock Wave Thermomechanical Processing of Aircraft Gas Turbine Disk Alloys," Pratt & Whitney Aircraft Final Technical Report, Contract N00019-78-C-0270, to Naval Air Systems Command, August 1979.

DISTRIBUTION LIST

(3 Copies)

Commander
Naval Air Systems Command (AIR-52031B)
Department of the Navy
Washington, DC 20361

(7 Copies)

Commander
Naval Air Systems Command (AIR-954)
Department of the Navy
Washington, DC 20361

AIR-954 (2 Copies)
AIR-536B1 (1 Copy)
AIR-330A (1 Copy)
AIR-330B (1 Copy)
AIR-5361A (1 Copy)
AIR-5362A (1 Copy)

(2 Copies)

Commander
Naval Air Development Center
Warminster, PA 18974

Code 606A (1 Copy)
Code 60634 (1 Copy)

(2 Copies)

Naval Air Propulsion Center
1440 Parkway Avenue
Trenton, NJ 08628

J. Glatz (PE-43) (1 Copy)
A. Martino (1 Copy)

Naval Sea Systems Command (Code 035)
Department of the Navy
Washington, DC 20362

Commander
Naval Weapons Center (Code 5516)
China Lake, CA 93555

Naval Ships Engineering Center (Code 6146)
Department of the Navy
National Center, Bldg. No. 4
Washington, DC 20362

DISTRIBUTION LIST (Continued)

Naval Ships Research & Development Center (Code 2812)
Annapolis, MD 21402

Commander
Naval Surface Weapons Center
White Oak
Silver Springs, MD 20910

Attn: Metallurgy Division

(2 Copies)

Director
Naval Research Laboratory
Washington, DC 20375

Code 6320 (1 Copy)
Code 6390 (1 Copy)

Office of Naval Research (Code 471)
The Metallurgy Program
Arlington, VA 22217

Naval Postgraduate School
Department of Mechanical Engineering (Code 69)
Monterey, CA 93940

Director
Army Materials and Mechanics Research Center
Watertown, MA 02172

Commanding General
U.S. Army Aviation Material Laboratories
Fort Eustis, VA 23604

(3 Copies)

Air Force Materials Laboratory
Wright-Patterson Air Force Base
Dayton, OH 45433

Code LLM (1 Copy)
Code LLN (1 Copy)
Metals Branch,
Manufacturing Technology
Division (1 Copy)

Air Force Aero Propulsion Laboratory
Wright-Patterson Air Force Base
Dayton, OH 45433

Code TB

National Aeronautics and Space Administration
Washington, DC 20546

Code RWM

DISTRIBUTION LIST (Continued)

(4 Copies)

National Aeronautics and Space Administration
Lewis Research Center
21000 Brookpark Road
Cleveland, OH 44135

C. M. Ault (1 Copy)
C. R. Halford (1 Copy)
Hugh Gray (1 Copy)
M. Hirschberg (1 Copy)

U.S. Department of Energy
Division of Reactor Research and Development
Mail Station B-107
Washington, DC 20545

A. Van Echo

Metals and Ceramics Information Center
Battelle, Columbus Laboratories
505 King Avenue
Columbus, OH 43201

AVCO RAD
201 Lowell Street
Wilmington, MA 01887

General Motors Corporation
Detroit Diesel Allison Division
Materials Laboratories
Indianapolis, IN 46206

General Electric Company
Aircraft Engine Group
Materials and Process Technology Laboratories
Evendale, OH 45215

United Technologies Research Center
400 Main Street
East Hartford, CT 06108

United Technologies Corporation
Pratt & Whitney Aircraft
East Hartford, CT 06108

Airesearch Manufacturing Company of Arizona
402 South 36th Street
P.O. Box 5217
Phoenix, AZ 85010

Attn: Chief, Materials
Engineering Dept.
Dept. 93-03M

AVCO Corporation
Lycoming Division
Stratford, CT 06497

DISTRIBUTION LIST (Continued)

Curtis Wright Company
Wright Aeronautical Division
Wood-Ridge, NJ 07075

Bell Aerosystems Company
Technical Library
P.O. Box 1
Buffalo, NY 14240

Solar
2200 Pacific Highway
San Diego, CA 92112

Dr. A. Metcalfe

Teledyne CAE
1330 Laskey Road
Toledo, OH 43601

TRW Equipment Laboratories
23555 Euclid Avenue
Cleveland, OH 44117

Mr. J. A. Alexander

General Electric Company
Corporate Research and Development
P.O. Box 8
Schenectady, NY 12301

M. G. Benz

Southwest Research Institute
8500 Culebra Road
P.O. Drawer 208510
San Antonio, TX 78284

G. R. Leverant

(27 Copies)

Commander
Naval Air Development Center
Warminster, PA 18974

A. Fletcher, Code 606A

(3 Copies)

Commander
Naval Air Development Center
Warminster, PA 18974

Code 8131

DAT
ILM